

	ORT	

DEVELOPMENT OF AN APPROACH FOR MEASURING THE TENSILE PROPERTIES OF ADDITIVELY MANUFACTURED LATTICE STRUCTURES

A T FRY, L E CROCKER, M J LODEIRO, H ZHANG, M POOLE, P WOOLLIAMS, A KOKO, C BREHENY¹

FEBRUARY 2024

¹ HiETA Technologies

DEVELOPMENT OF AN APPROACH FOR MEASURING THE TENSILE PROPERTIES OF ADDITIVELY MANUFACTURED LATTICE STRUCTURES

A T FRY, L E CROCKER, M J LODEIRO, H ZHANG, M POOLE, P WOOLLIAMS, A KOKO, C BREHENY¹

Advanced Engineered Materials

¹HiETA Technologies

© NPL Management Limited, 2024

ISSN 1754-2979

https://doi.org/10.47120/npl.MAT127

National Physical Laboratory Hampton Road, Teddington, Middlesex, TW11 0LW

This work was funded by the UK Government's Department for Science, Innovation & Technology through the UK's National Measurement System programmes.

Extracts from this report may be reproduced provided the source is acknowledged and the extract is not taken out of context.

Approved on behalf of NPLML by Stefanos Giannis, Science Area Leader.

CONTENTS

1	INTRO	DDUCTION	1
2	REVIE	CW OF SPECIMEN DESIGN AND MANUFACTURE	1
3	MECH	IANICAL TESTING	6
	3.1 MAC	ROMECHANICAL	6
	3.1.1	Universal Test System	6
	3.1.2	Universal Test System Results	8
	3.1.2.1	Single Ligaments	8
	3.1.2.2	Lattice Structures	14
	3.2 MICR	ROMECHANICAL TESTING	25
	3.3 NANO	OMECHANICAL TESTING	29
4	FINIT	E ELEMENT MODELLING	33
	4.1 SING	LE LIGAMENT MODEL	33
	4.2 LATT	TICE MODEL	37
5	DISCU	SSION	50
6	REFEI	RENCES	51

1 INTRODUCTION

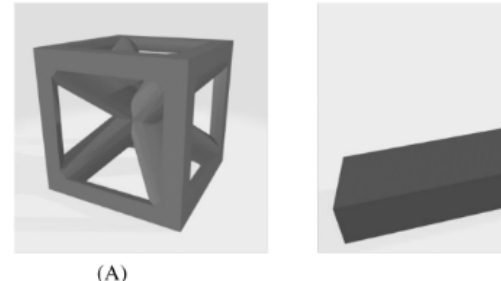
Due to inherent variability of the additive manufacturing (AM) process, it is understandable that that manufacturers are concerned with the consistency of components and are looking for appropriate test methods to help characterise, validate, and provide quality assurance.

Within the manufacturing industry there is a growing use and application of lattice or porous designs which is afforded by the design flexibility that AM offers. As with bulk AM processing there is variability and different manufacturing systems will inevitably exhibit different capabilities in terms of resolution of features as well as resultant strength. Lattice structures have the capacity to generate unique mechanical, electrical, thermal and acoustic properties (1). There has been a large amount of information published relating to the mechanical properties of these structures. Generally, the mechanical testing of SLM lattices has been performed under compression and work has been progressing on the development of a standard test artefact and approach (2). This form of testing for lattices is relatively more straightforward to carry out and analyse than tensile testing. The compression test can be simply performed by compressing an as-manufactured lattice between two platens. When testing in tension there are more challenges to overcome, for example how to attach the lattice structure to the testing apparatus. It has been reported that this area of the test piece is critically important, and that this region can be responsible for premature failure due to stress concentrations at the interface (3).

The need for materials measurement and validation requires the development of standardised coupons that may be used as a surrogate in destructive evaluations. Since each lattice design is potentially different for all manufacturers, a standardised approach is needed to ensure that the lattice design is adequately represented and can be consistently assessed. The work presented in this report describes such an approach and builds on the work previously reported in NPL report MAT 119 (4), extending it from simple single ligands to more complex lattice structures.

2 REVIEW OF SPECIMEN DESIGN AND MANUFACTURE

There are several different design approaches taken in the literature to facilitate tensile testing of lattices. These have tended to focus on quite large multi-cellular lattices as illustrated in Figure 1. The specimens have a cross-sectional area of 4 x 4 cells (around 10 x 10 mm) with four cells in height that have constant density at the lattice centre and two layers of cells either side closest to the grips with graded density, in order to smooth the transition between the lattice and the grips and to localize failure in the central region. A graded density was obtained by linearly increasing the struts diameter, from 0.6 to 0.8 mm in the layer closest to the lattice centre and from 0.8 to 1.2 mm in the next layer, closest to the grips (5). The approach within our work was to start at a very basic level, measuring the tensile strength of a single ligand. Develop the finite element model for this ligand and then scale up to a single lattice unit cell. Validate the model response against this unit cell and then increase in scale to larger lattice constructs. The initial part of this work has been previously reported in NPL Report MAT 119 (4) and so will only be briefly reviewed.



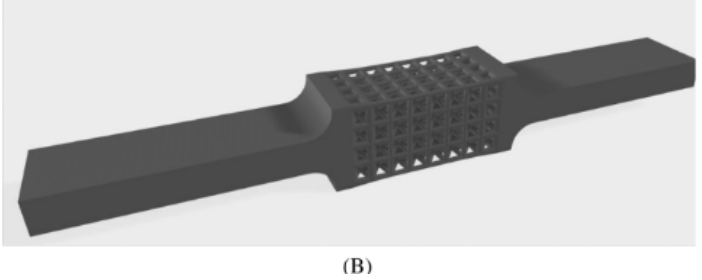


Figure 1 SC-BCC unit cell (A) and specimen geometry (B) with graded density to smooth transition between lattice and grips, used for monotonic tension and compression tests (5)

It was important, in order to be able to realise this work, that the specimen design could be tested in a range of equipment and did not require specially developed mounts or grip systems. There was a conscious decision therefore to ensure that the sample could be both gripped in wedge action grips which are commonly found on universal test systems and could also be gripped with a simple plate system secured using bolts, a system commonly found in apparatus for small scale sample testing. The design took inspiration from an approach used in single fibre testing where the fibre is usually supported by some form of framing support material that can be disconnected from the load chain after gripping the specimen but before full test loading, thus preventing premature failure of the fragile samples during the gripping stage.

There were two specimen forms that were of interest in this work. The first was the lattice struts or ligaments which form the long axis of the lattice unit cells connected by nodal points. The second form was the lattice unit cell itself, consisting of a minimal number of lattice cells within this phase of the work.

The ligand sample was made by combining the required cylindrical gauge length to two rectangular grip sections (1 mm thick, 10 mm wide and at least 20 mm long) and then blending the gauge into the grip sections to give a smooth transition. The gripping portion of the test pieces extended to a sufficient length to ensure adequate gripping area for a variety of gripping solutions and test systems. The grip section also provides the end user with the ability to include markers to identify the samples. In the example shown in Figure 2, indents have been manufactured in the top and bottom end tabs. IDs can also be manufactured onto the end of the specimen if necessary.

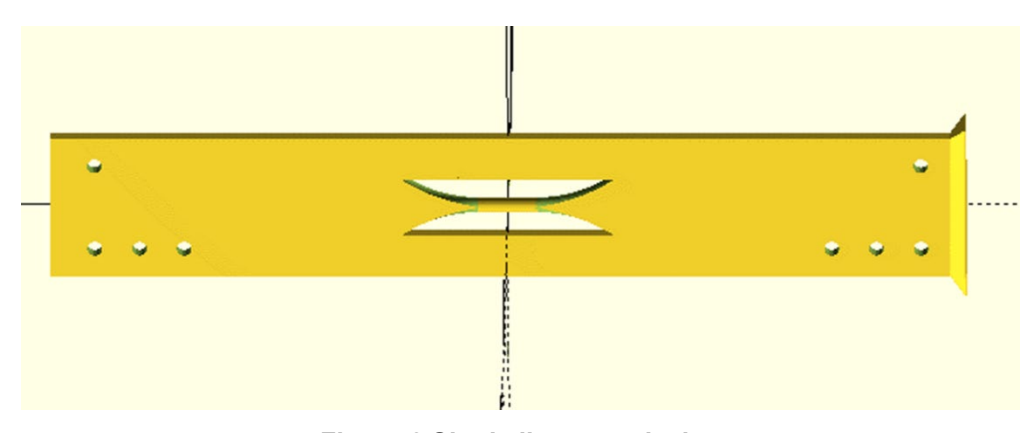


Figure 2 Single ligament design

To either side of the ligament piece are two thick supporting bars, each 3 mm wide, which bridge across the top and bottom half of the test piece. These provide strength and support to the top half of the test piece and to protect the ligament during manufacture and powder removal, as well as protection from any applied load during the mounting of the test piece into the universal test machine prior to testing. Once in position the side supports can be simply but carefully cut through with a grinding tool (such as a Dremel ®) or with a fine hacksaw.

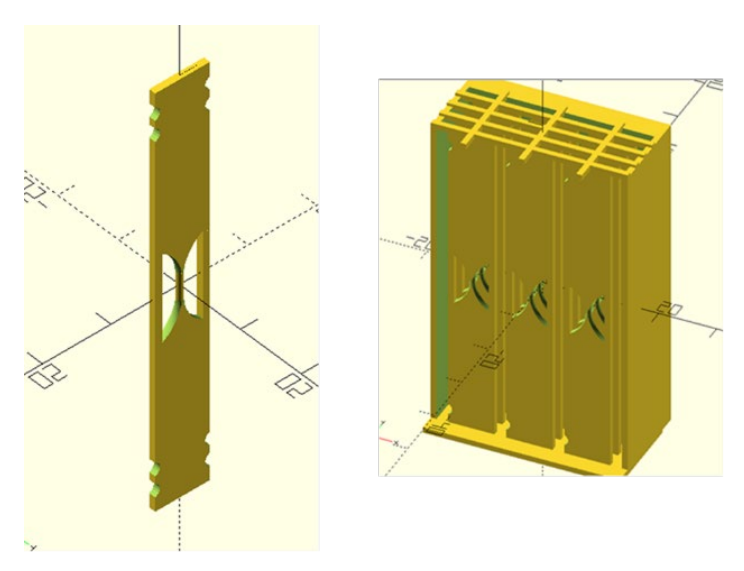


Figure 3 Design of single ligament test specimen and multiple specimen cassette

To further protect the test piece during manufacture, handling and transport, a cassette design was used to allow numerous samples to be manufactured and held together in a spur-type configuration. This is shown on the right-hand side of Figure 3. The test pieces are manufactured in a grid and then encased on all four sides by a solid wall of material locally punctuated with holes for post-manufacture processes.

For example, for the 1 mm diameter samples four test pieces were arranged together for each of the four gauge lengths equalling 1, 2, 3 and 4 multiples of the ligament diameter (so 1, 2, 3 and 4 mm gauge lengths in this case) providing 16 samples in total, Figure 4. In order to efficiently pack these together into a single build cassette, the maximum sample length was found (in this case for the samples with gauge length equivalent to 4 times the diameter) and the grip sections for the 1, 2 and 3 times samples were made commensurately longer so all the samples had the same overall length. Chamfers were added to the top and bottom to aid building. Finally, a solid base was added, and a thin 1 mm thick wall surrounded all the samples, with holes through the side to allow powder removal and identification of the block. This approach was repeated for ligament diameters of 0.5 amd 0.75 mm.

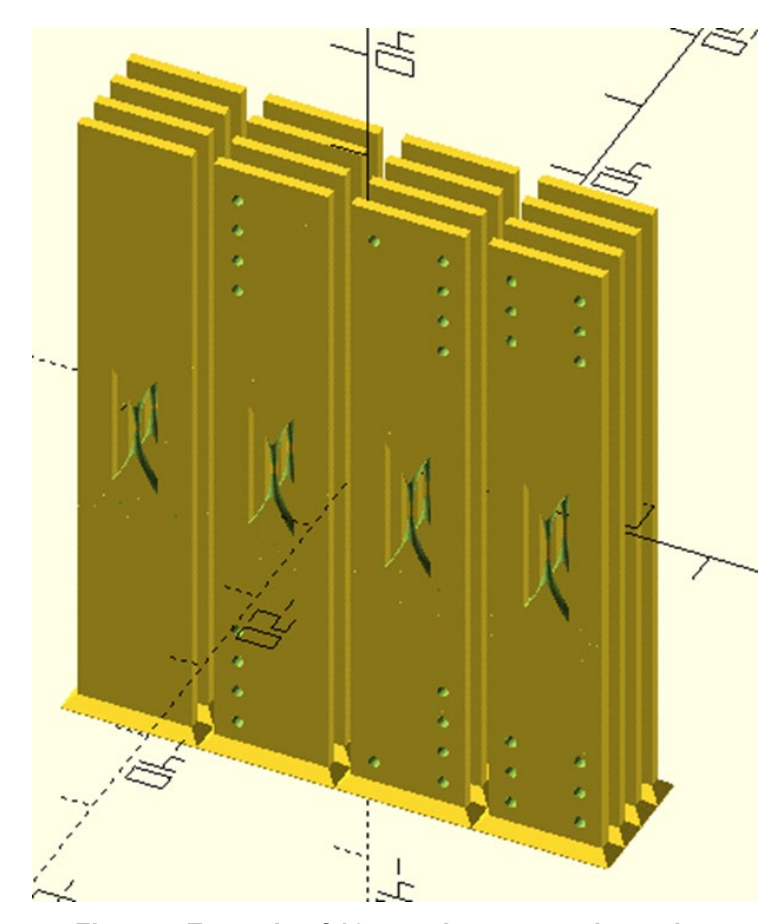


Figure 4 Example of 16 samples arranged together

Examples of the actual cassettes can be seen in Figure 5 showing cassette builds at different angles to the build plate with corresponding support structure. The samples were made either vertically or with an additional angled base block so that the samples were built with an angle of 35.6° from the horizontal.

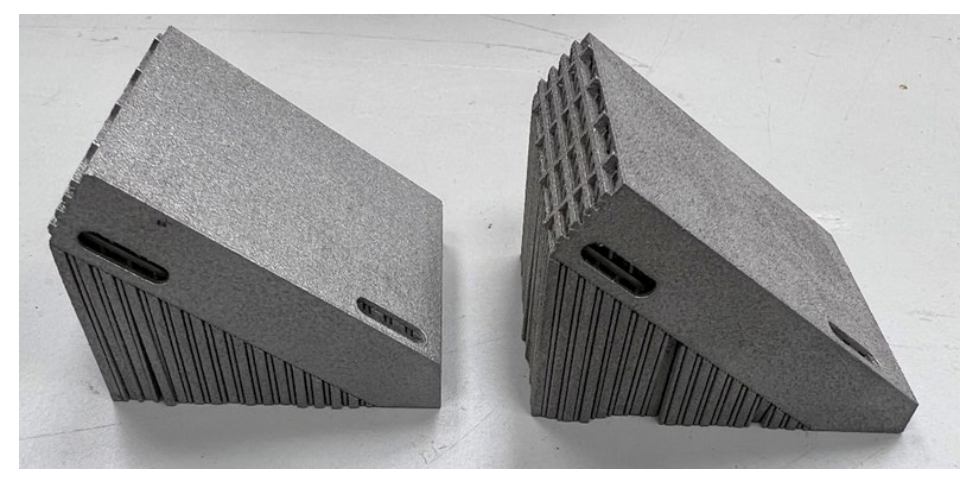




Figure 5 Example of cassette design showing the holes in the side walls for powder removal purposes

Having developed a test piece design and manufacturing approach, the design was extended for use with lattice cells, as shown in Figure 6. This shows a single line consisting of nine lattice cells attached to grip sections, keeping consistent with the single ligament sample. As before the main test piece is protected from accidental or premature damage by side supports.



Figure 6 Example of a lattice test piece

All test pieces were manufactured from AlSi10Mg powder using a laser powder bed manufacturing route on a Renishaw 500Q.

3 MECHANICAL TESTING

3.1 MACROMECHANICAL

3.1.1 Universal Test System

Tensile tests were conducted using an Instron 5969 universal mechanical test machine fitted with a 50 kN load cell. The coupons were gripped using a pair of wedge action grips fitted with serrated grip faces. The alignment of the test machine and grips was set prior to testing the ligaments by gripping a stiff steel bar and loading to 1 kN before firmly locking the position of the grips. The test pieces were loaded for initial tests at a crosshead speed of 1 mm per minute until failure.

Prior to testing, the test pieces were speckled using white and black spray paints. Strain was subsequently measured on opposing faces of the test piece using a non-contact video extensometer (Imetrum ®). The test setup is illustrated in Figure 7, showing the test piece gripped in the wedge action grips and the two cameras imaging the front and back face of the test piece for non-contact strain measurement. A closer view of the test piece in the grips is given in Figure 8.

The non-contact strain measurement method allows strain to be measured in several different ways from a single dataset. The user can use a full field approach and measure the strain over the whole gauge length, or multiple discrete areas can be selected allowing the user to simulate a standard strain gauge measurement, or markers combined with a video extensometer approach can be employed. An example of the images captured is shown in Figure 9.



Figure 7 Instron universal test machine setup used for testing with cameras imaging front and back faces of the test piece simultaneously for strain measurement



Figure 8 Single ligament test piece held in wedge action grips

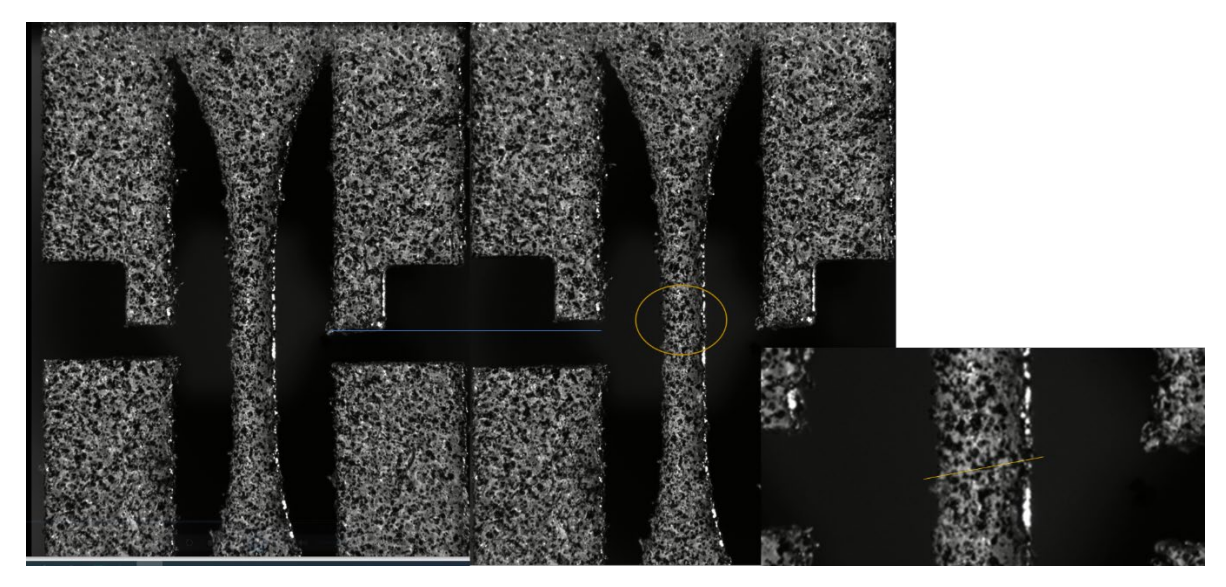


Figure 9 Captured frames from the Imetrum video of a test showing the initial frame (far left) final frame (middle) and a closeup of the failure in the final frame with the fracture marked by the yellow line (far right)

3.1.2 Universal Test System Results

3.1.2.1 Single Ligaments

Initial tests were conducted on the 1 mm diameter samples. The results of the tests on the 1 mm diameter ligament samples with a gauge length of 2, 3 and 4 mm were presented in (4) and the load vs displacement data summarised in Figure 10. The stress has been calculated using an assumed diameter of 1 mm, this is a nominal value as the material was tested in the as-manufactured condition and so some surface roughness will be present. This can be seen in Figure 11 which shows one of the ligament test pieces imaged in the Starrett MVR 300 optical measurement system. This image also shows the speckle pattern on the test piece. From Figure 11 it can be seen that there are surface asperities on the gauge length. Measured optically, the minimum diameter was found to be 1.070 mm, the maximum value was 1.081 mm and the mean value was found to be 1.076 mm. The plot of stress against strain is shown in Figure 12. This shows that repeatability between the three measured samples with the same nominal geometry is very good. Further repeat measurements were conducted on the single ligament test pieces to determine the degree of variability in the material properties and the effect of test rate, reduced in these instances to 0.1 mm/min, presented in Figure 13.

Whilst there is some scatter in the load-displacement curves, when the data is plotted as stress against strain the curves converge, as shown in Figure 14. Apart from one outlier (2AJIN002) the rest of the repeat measurements follow the same curve up to the yield point, after which they start to diverge and finally fail at elongations of 11% to 24.5% average strain. Note that the strain is reported in Figure 14 as an average because the front and rear face of the sample was observed with the Imetrum ® non-contact strain system, and it is the average of these two values that has been used. The two-sided imaging enables bending in the test piece to be monitored, which can often help to explain unexpected scatter in the results.

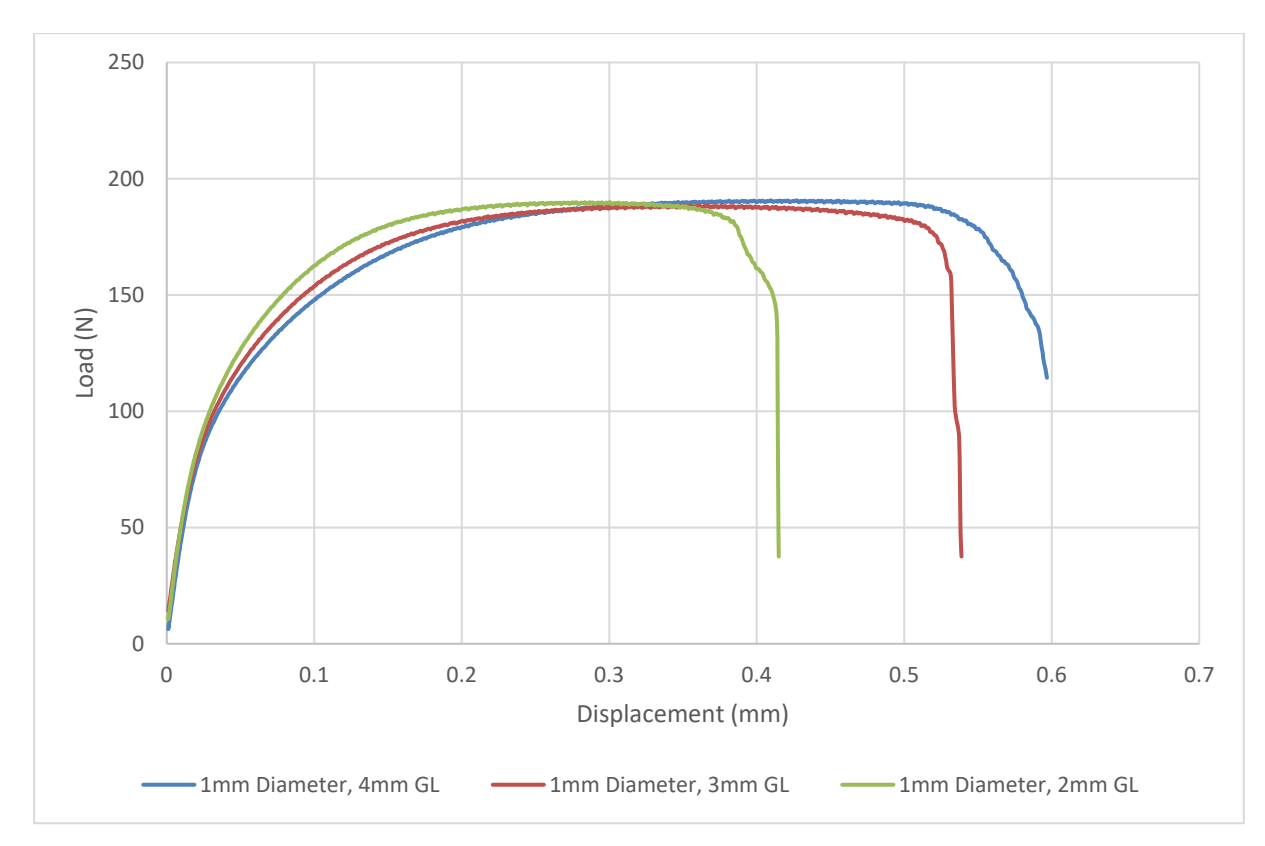


Figure 10 Load vs displacement results for the 1mm diameter single ligament samples

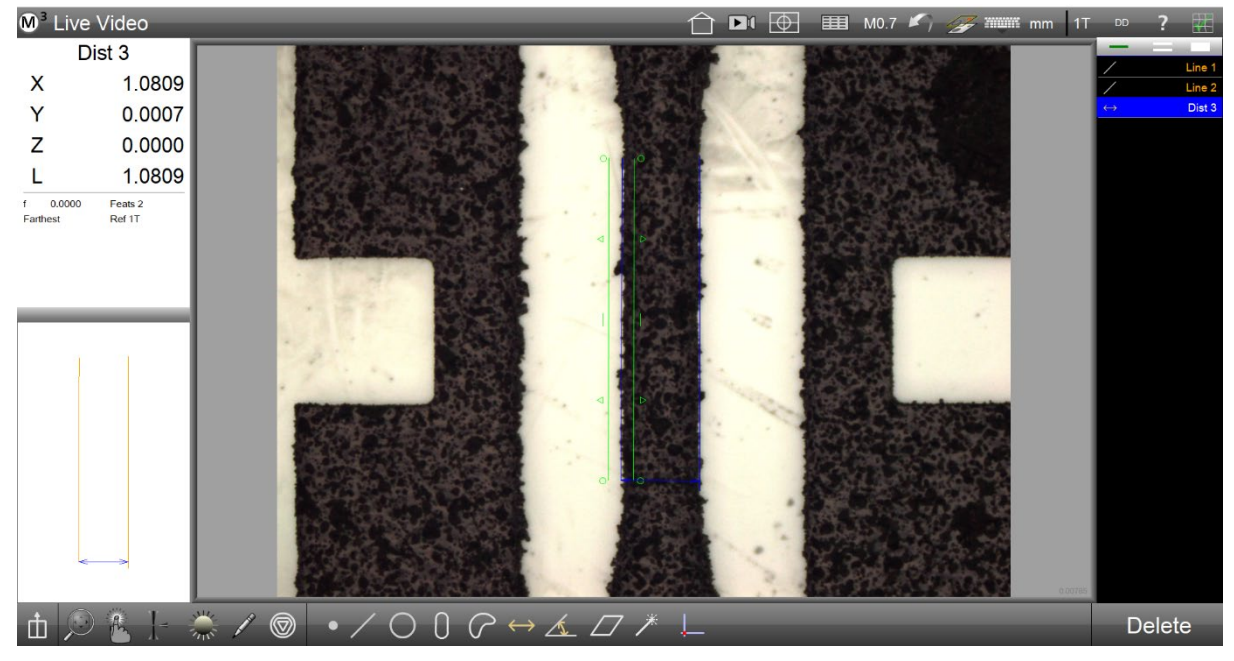


Figure 11 Image from the Starrett MVR 300 optical measurement system

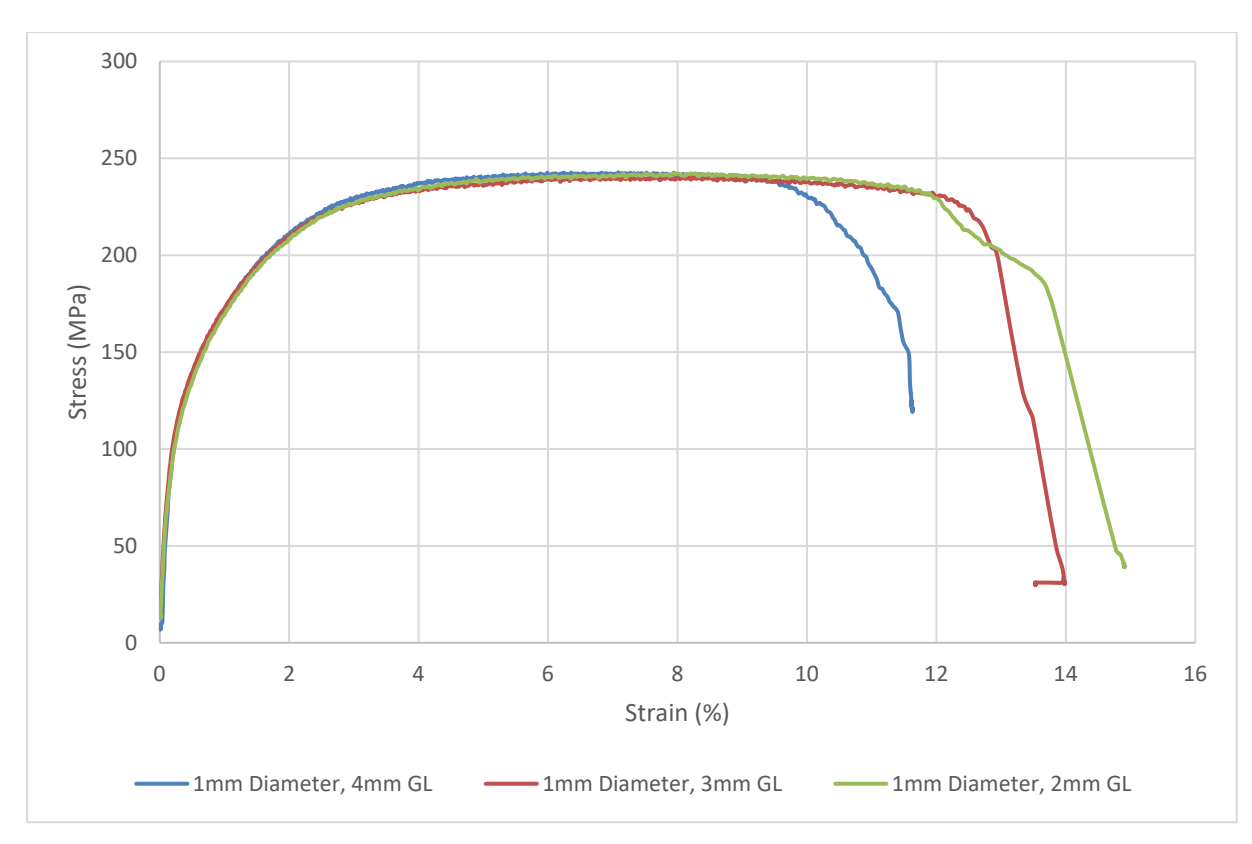


Figure 12 Stress vs strain results for the 1 mm diameter single ligament samples

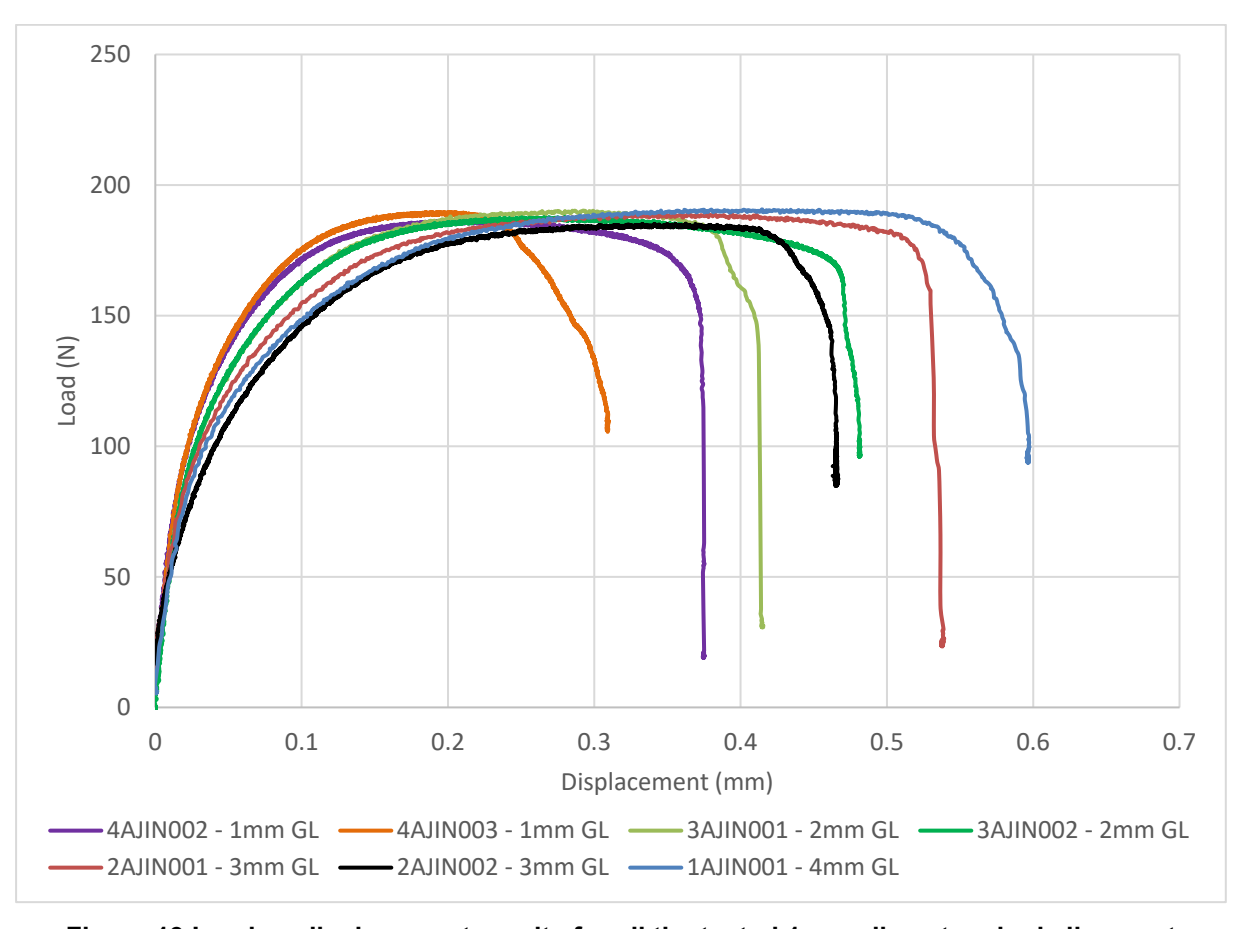


Figure 13 Load vs displacement results for all the tested 1 mm diameter single ligament samples

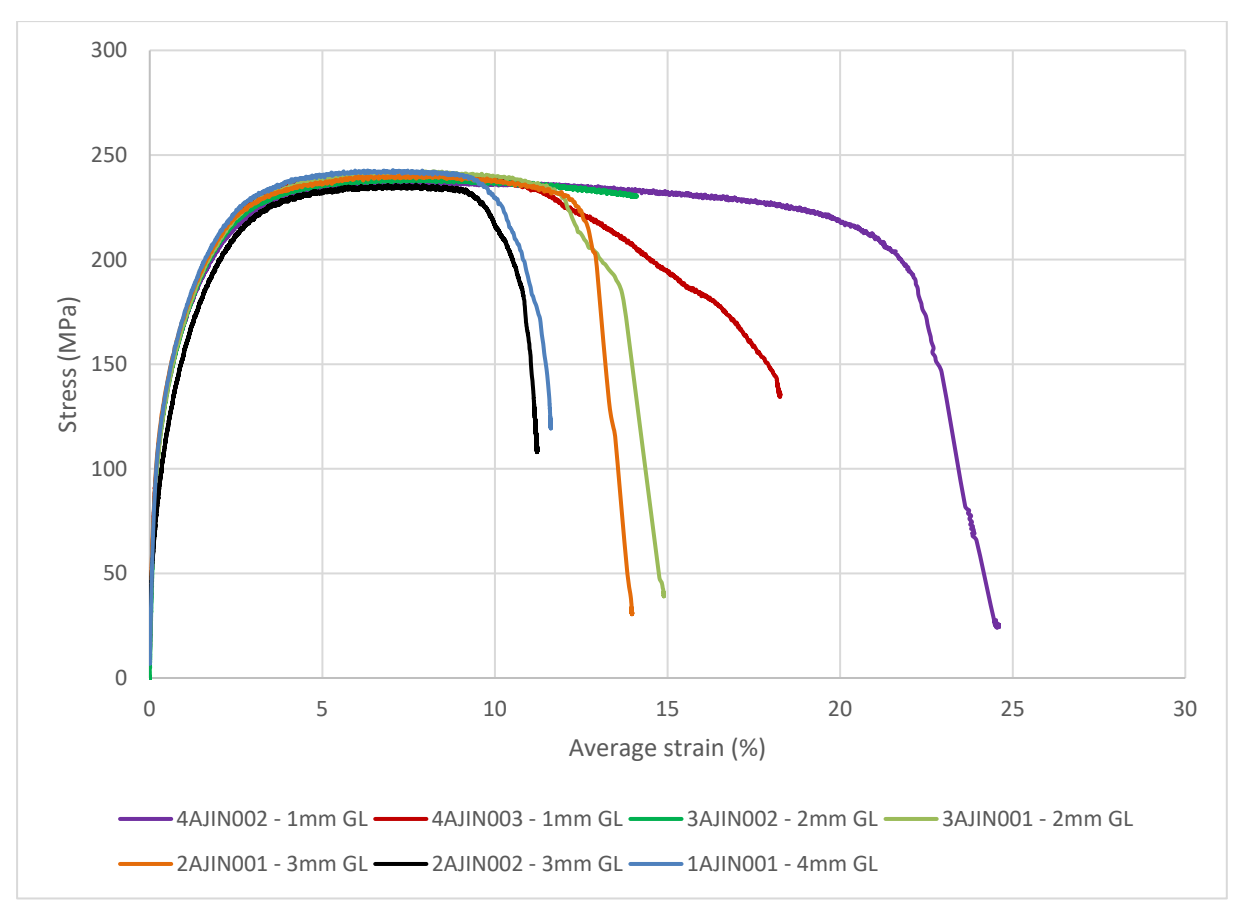


Figure 14 Stress vs average strain results for all the tested 1 mm diameter single ligament samples

The results of the analysis of the stress-strain data from these initial tests are presented in **Table 1**, which shows the elastic modulus, yield stress and ultimate tensile stress values.

Table 1 Summary results for the single ligament tensile tests

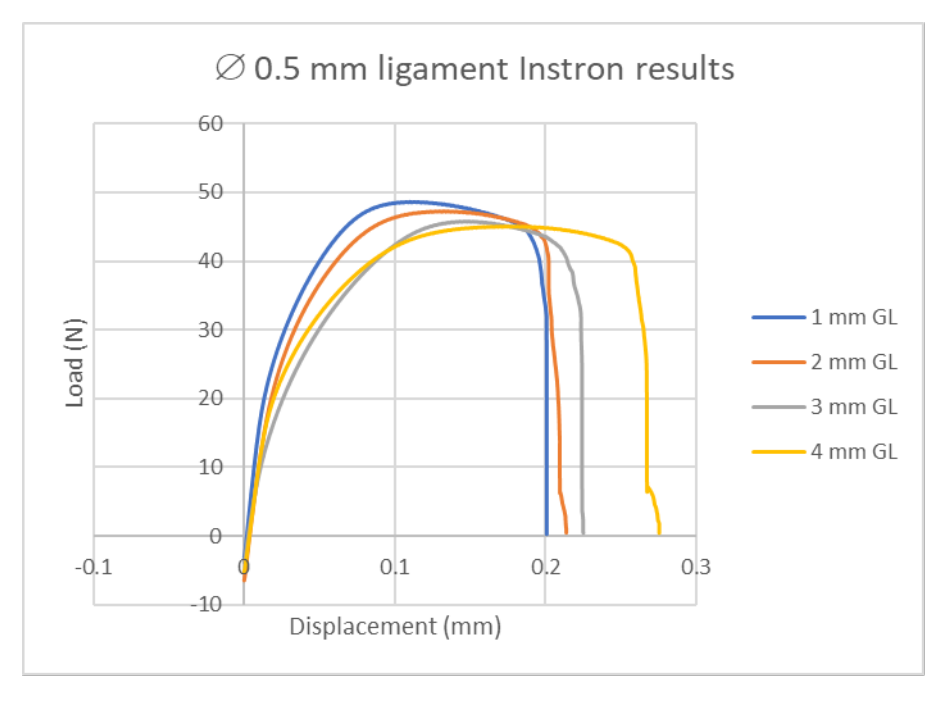
Sample ID	Elastic	Yield Stress,	Ultimate Tensile	Sample Gauge
	Modulus*, GPa	MPa	Stress, MPa	Length, mm
1AJIN001	69.0	128.5	242.8	4
2AJIN001	67.4	130.7	240.4	3
3AJIN001	64.3	125.5	242.5	2
2AJIN002**	40.9	116.1	235.9	3
3AJIN002	71.5	124.7	239.1	2
4AJIN002	70.3	124.8	237.8	1
4AJIN003	72.0	126.8	241.5	1
Average	69.08	125.3	240	
Standard	2.88	4.60	2.54	
Deviation				
Coefficient of	0.04	0.04	0.01	
Variation				

^{*} calculated over a strain range of 0.01 to 0.05% for a nominal 1 mm ligament diameter

Further tests have been conducted on 8 different ligament geometries, these were 0.5 and 0.75 mm diameter ligaments with length of 1, 2, 3 and 4 mm. The load vs displacement plots

^{**} outlier and excluded from modulus calculations

for these tests are presented in Figure 15. Figure 16 shows the load vs displacement results for all the three different ligament diameters. The corresponding stress vs strain plots for the 0.5- and 0.75-mm diameter ligaments are shown in Figure 17.



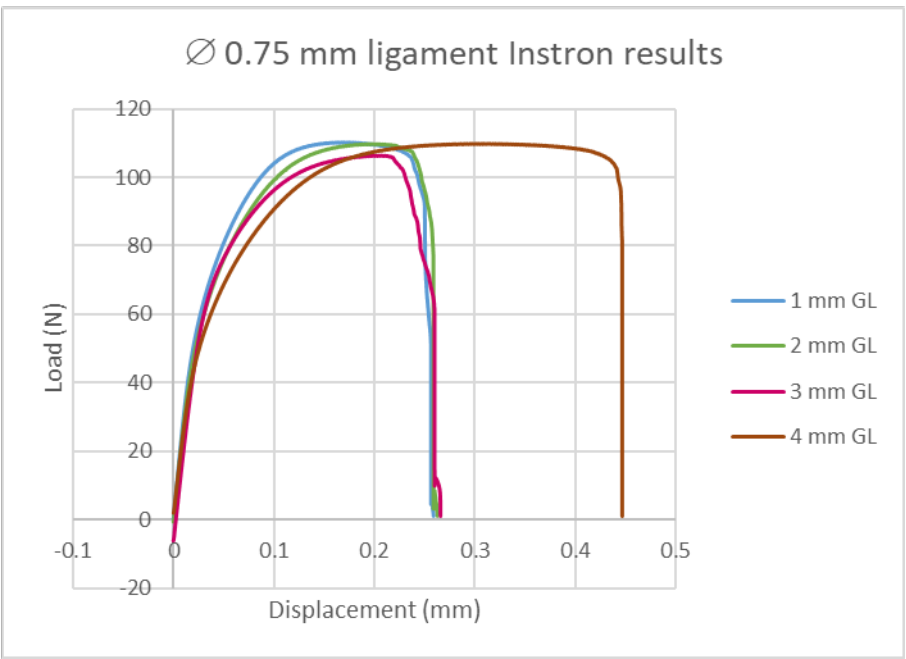


Figure 15 Load vs displacement results for all the tested 0.5- and 0.75-mm diameter single ligament samples

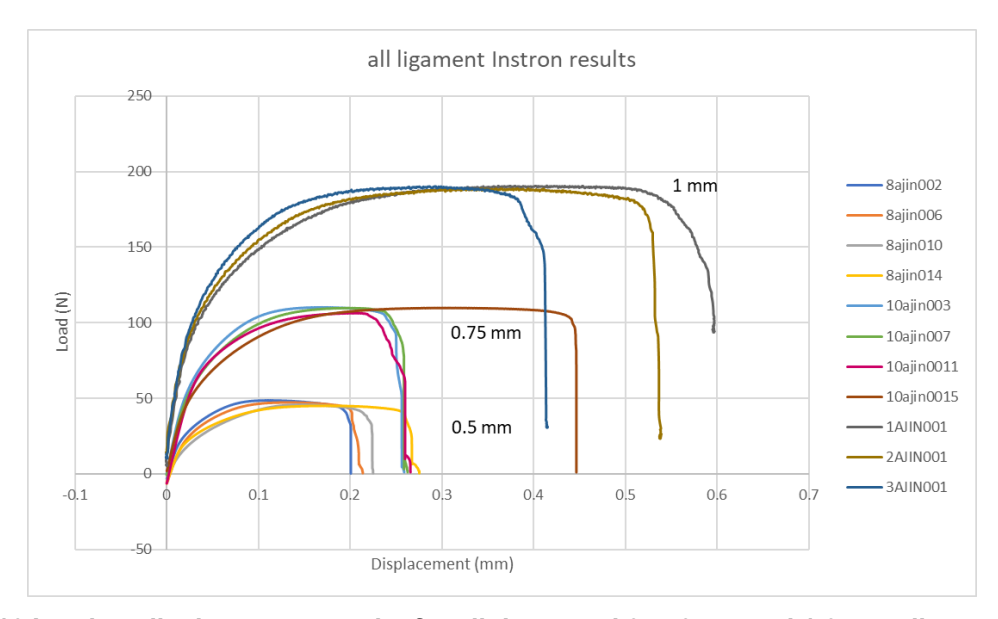
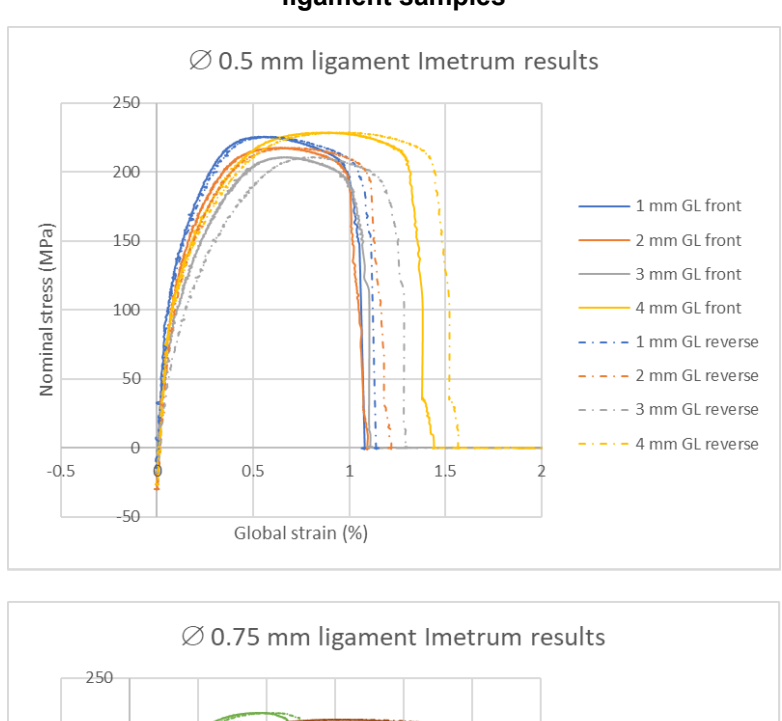


Figure 16 Load vs displacement results for all the tested 0.5, 0.75- and 1.0-mm diameter single ligament samples



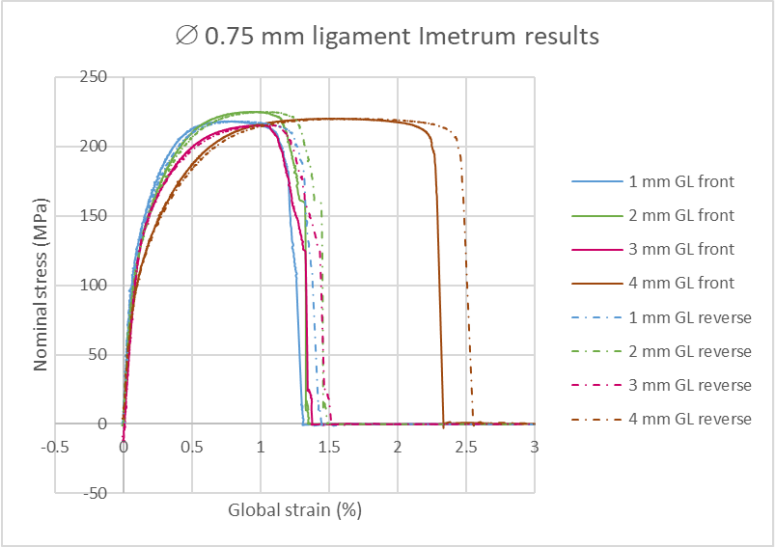


Figure 17 Nominal stress vs global strain results for all the tested 0.5- and 0.75-mm diameter single ligament samples

A comparison of the nominal stress (nominal as the exact cross-sectional area is not measured) vs the global strain (global as the strain is measured between the two gripping sections) can not be made as the gauge length over which the strain was measured was different for the previous 1 mm diameter ligament samples. Figure 18 shows the relationship between maximum load and the ligament diameter.

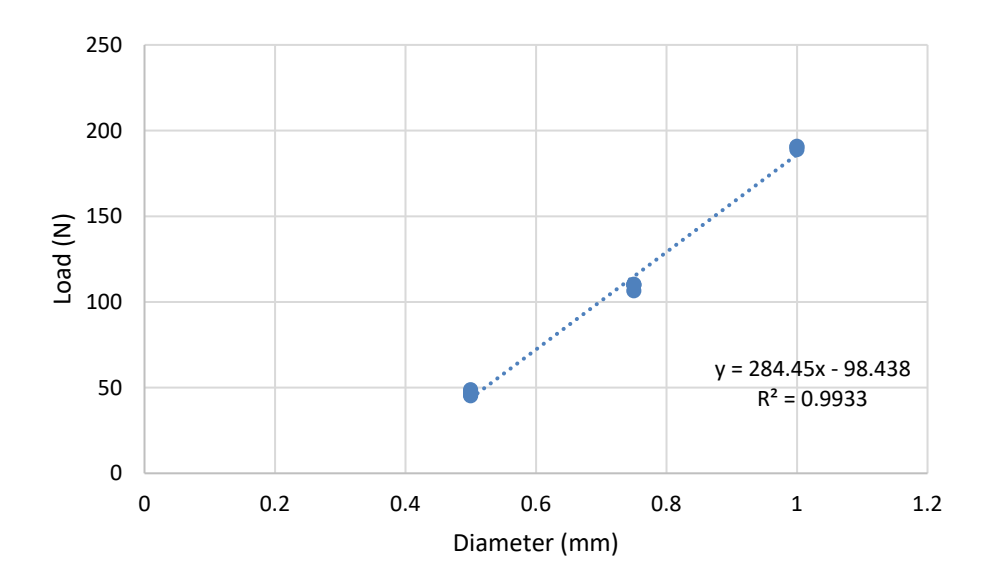


Figure 18 Maximum load vs ligament diameter

The measurements conducted on the single ligament samples with different diameters and lengths showed:

- That the test method could produce repeatable results as demonstrated from the modulus, yield and UTS values tabulated in Table 1 for the 1 mm diameter ligament with gauge lengths (sample lengths) from 1 mm to 4 mm.
- As expected, as the diameter of the ligament is reduced so does its load bearing capacity. The reduction in the maximum load is approximately 50% per 25% reduction in diameter.
- When considering the ultimate tensile strength of the ligaments the average value for all the sample tested was found to be 220 MPa, with maximum and minimum values of 228.6 MPa and 210.8 MPa respectively.
- Elongation to failure was generally found to increase with increasing gauge length.

3.1.2.2 Lattice Structures

The same test piece design was adopted for the lattice unit cell samples. The aim was to measure the strength and mechanical properties of a single lattice cell before scaling up into more elaborate structures. Initially the focus was on one unit cell, and to facilitate this the test pieces were manufactured in a chain of nine cells. Two different strut diameters were used 0.30 mm and 0.25 mm as shown in Figure 19, using a relatively simple BCC unit cell geometry. The 0.25 mm lattices were formed from a chain of 3 cells of 0.3 mm diameter at each grip end for strength with the central 3 unit cells reduced to 0.25 mm diameter. Testing was conducted in the universal test system using a displacement rate of 0.1 mm/min using a 1 kN load cell. As with the single ligament test piece, the sample was very carefully mounted and gripped into the test machine (this was done without specimen protect engaged as this feature was causing jitter as the system struggled to control at low load levels) before the side supports were cut through. Repeat tests were conducted on the two lattice designs (0.3 mm and 0.25 mm

diameter) and an example of the results, showing applied load and displacement, are provided in Figure 20. This shows that as expected the larger lattice struts were able to carry higher loads reaching ~32 N, whilst the thinner struts were only able to carry ~8.5 N. An approximation has been made of the load bearing cross sectional area of the lattice, based on the nominal strut diameter, and the corresponding stress calculated for each test. The plot of nominal stress vs displacement is shown in Figure 21, with the 0.3 mm lattice struts plotted on the left-hand axis and 0.25 mm strut on the right-hand axis. This shows that yield for the two lattice structures occurred at a similar applied displacement and that the 0.3 mm lattice had an ultimate tensile strength (UTS) of 112 MPa and the 0.25mm lattice a UTS of 42.7 MPa. Non-contact strain measurement (Imetrum) was used during these tests setting the gauge length markers over three distinct regions. The first was to consider the 'global' strain on the test piece by considering the gauge length to be the point between the lattice and the end tab section, shown in Figure 19 as the yellow lines. The second gauge length considered a reduced range closer to the expected failure, either the central 5 unit cells for the 0.3 mm struts or the central 3 unit cells for the 0.25 mm struts, shown in Figure 19 as the red line. Finally, the third region considered the central 3 unit cells for the 0.3 mm diameter struts or the single central unit cell for the 0.25 mm diameter struts, shown in Figure 19 as the green line.

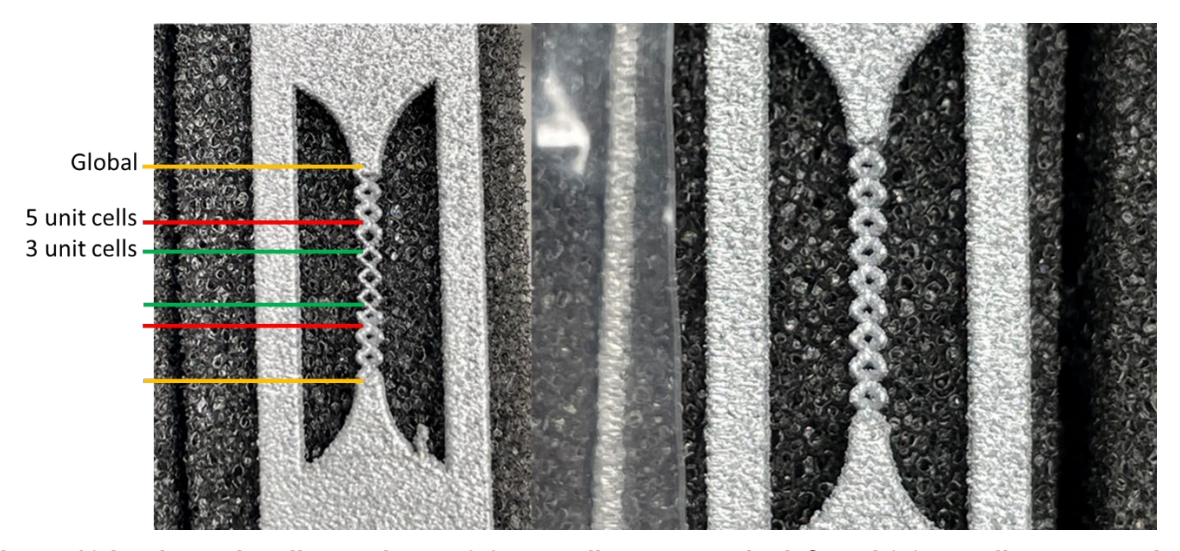


Figure 19 Lattice unit cell test pieces, 0.25 mm diameter on the left and 0.3 mm diameter on the right

All the result plots (Figure 20 to Figure 23) show a stepped failure of the lattice test piece. Observation of the lattice structure during the tests showed that failure was not apparent across the whole lattice structure with little obvious elongation or deformation on the adjacent unit cells beyond the one that ultimately resulted in failure. This can be seen in Figure 24 and Figure 25, which show the failed specimens for the 0.3 mm and 0.25 mm lattices respectively.

Deformation and final failure are focussed on a single lattice unit cell, as one might expect for this particular layout and geometry, with failure occurring in one lattice strut after the other until the whole sample fails. The actual failure location with the lattice cell was seen to vary, with failure occurring in the centre section of a strut in some cases whilst others would fail closer to the node or apex.

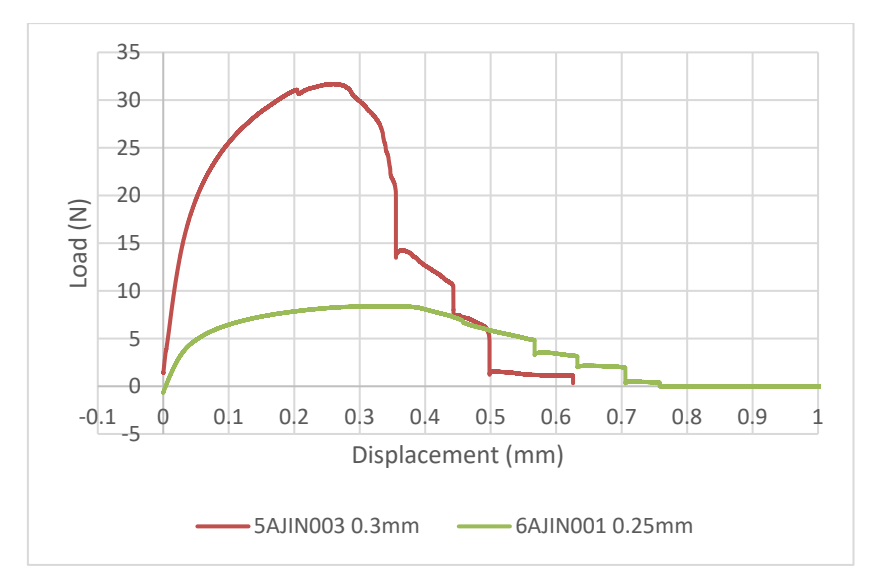


Figure 20 Load vs displacement for the 0.3 mm and 0.25 mm lattice test pieces

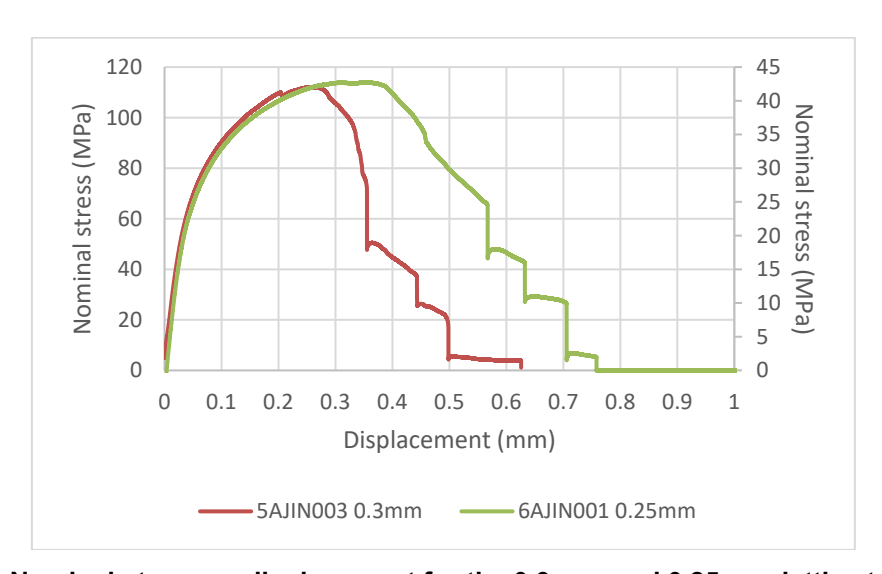


Figure 21 Nominal stress vs displacement for the 0.3 mm and 0.25 mm lattice test pieces

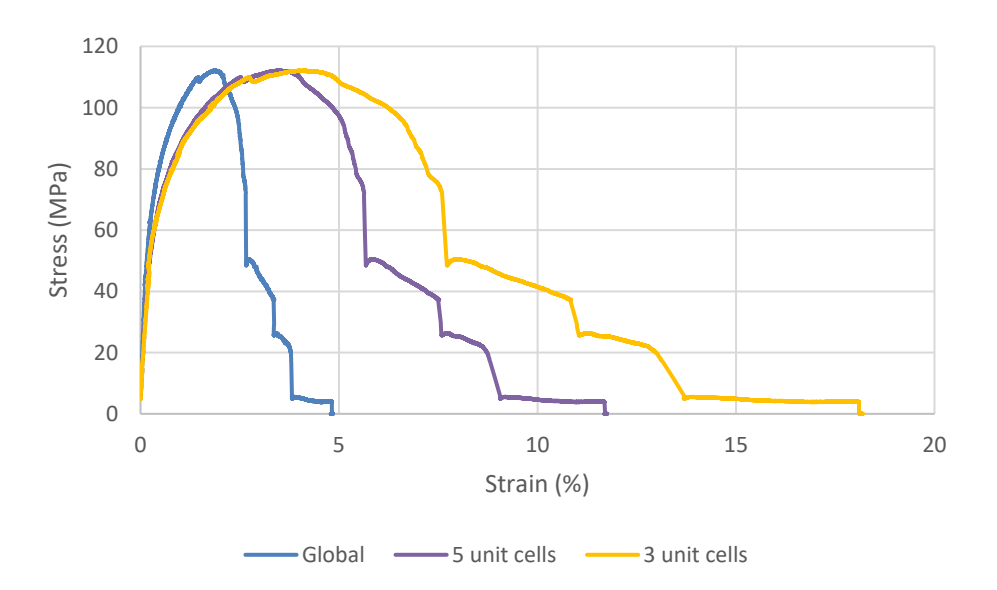


Figure 22 Nominal stress vs strain plots for the 0.3 mm diameter lattice test piece with the strain measured by the Imetrum over different gauge length ranges

Figure 22 shows the stress vs strain response for the 0.3 mm lattice. In this case the failed lattice cell was within the smallest analysis field of view of the Imetrum, and so in each of the traces we observe the sequential failure of the lattice struts. This is not the case with the 0.25 mm diameter lattice test piece shown in Figure 23. In this case the global and 3 unit cell analysis windows capture the failure instances, but the central unit cell was not the failure cell and only shows the elastic/plastic response of a lattice cell without the sudden strain increases seen in the other two traces. The failed lattice cell in each instance is shown in Figure 24 and Figure 25. It is particularly evident in Figure 25 that the failed lattice cell has undergone extensive elongation and 'straightening' of the cell compared to the cells in the chain above and below it.

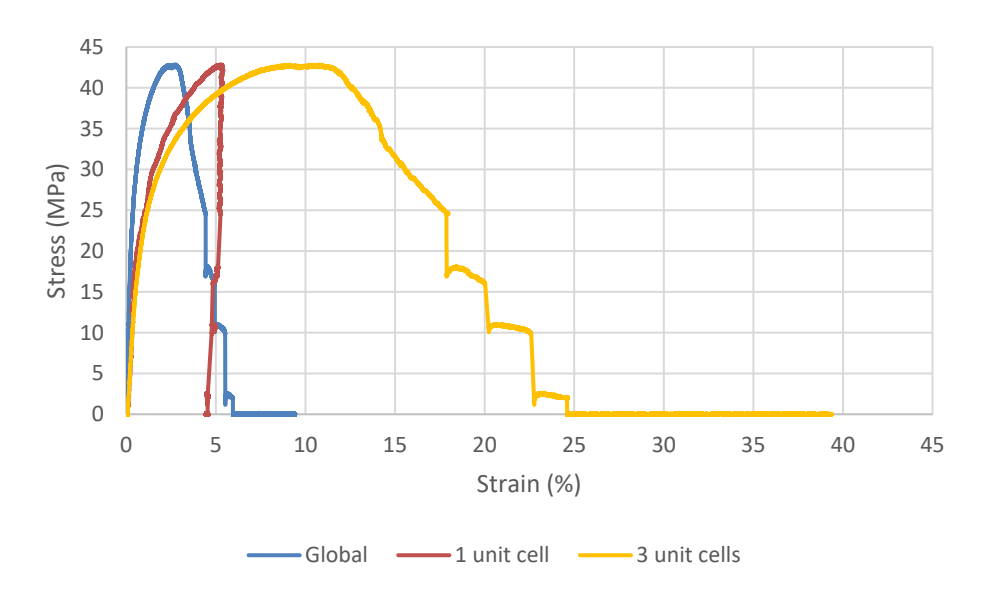


Figure 23 Stress vs strain plots for the 0.25 mm diameter lattice test piece with the strain measured by the Imetrum over different gauge length ranges



Figure 24 0.3 mm lattice test piece after testing

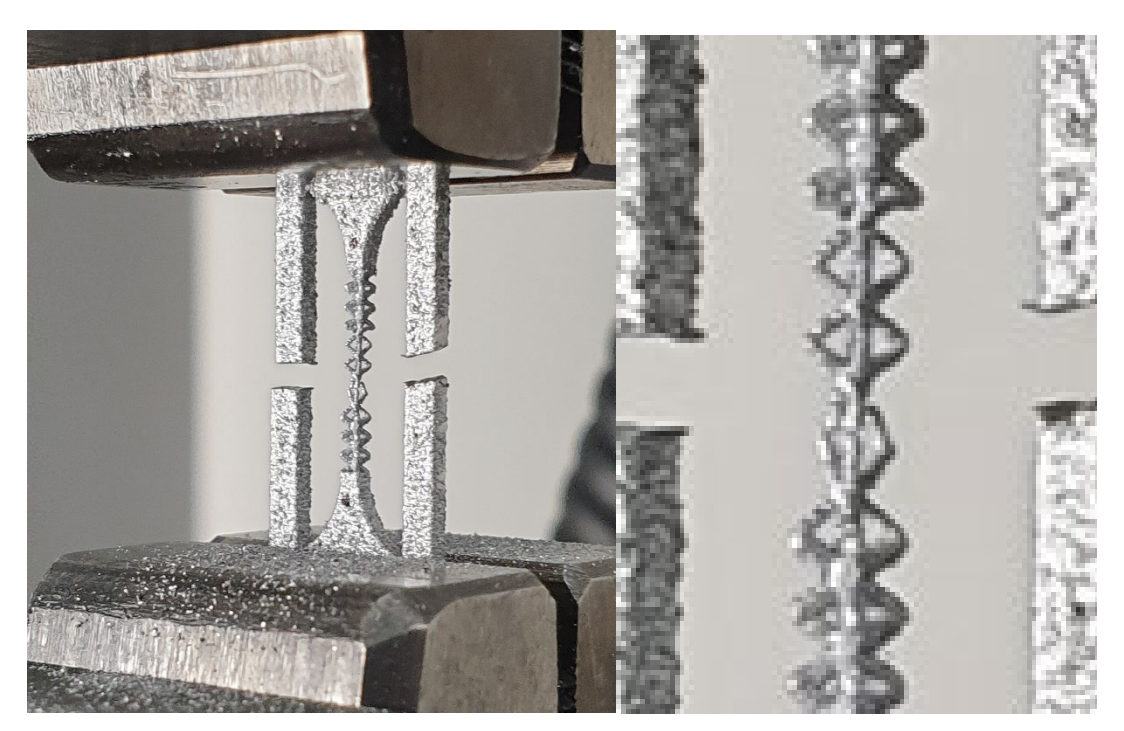


Figure 25 0.25 mm lattice test piece after testing

A second batch of lattice samples were manufactured with a 0.4mm diameter ligament. Samples were supplied in the following geometries:

- 1 x 1 x 9 cells
- 2 x 1 x 9 cells
- 5 x 1 x 9 cells

Tensile testing was conducted following the same procedure as detailed above. Figure 26 shows two test pieces after tensile testing. The figure shows that the failure is constrained to one cell centrally located in the lattice chain, as with previous samples.



Figure 26 0.40 mm 1 x1 x 9 lattice test pieces after testing

The load vs displacement and nominal stress vs global strain are shown in Figure 27 and Figure 27 respectively. These figures show the sequential failure in the lattice unit cell as previously described for the larger lattice strut diameter. The failure incidents occur with broadly similar drops in load and corresponding nominal stress. Compared with the smaller 0.25- and 0.3-mm diameter lattice struts the actual failure stress is similar for all samples. Note that the failure strain (measured using the global parameter) is also broadly in agreement between the three sample sizes, with a strain of around 3% being achieved.

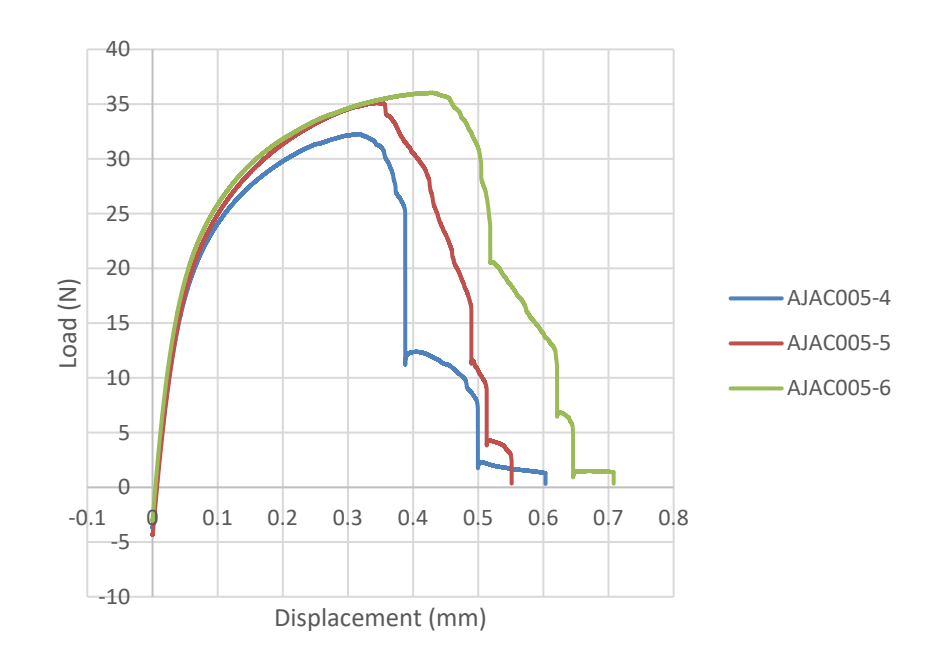


Figure 27 Load vs displacement results for 0.40 mm 1 x1 x 9 lattice samples

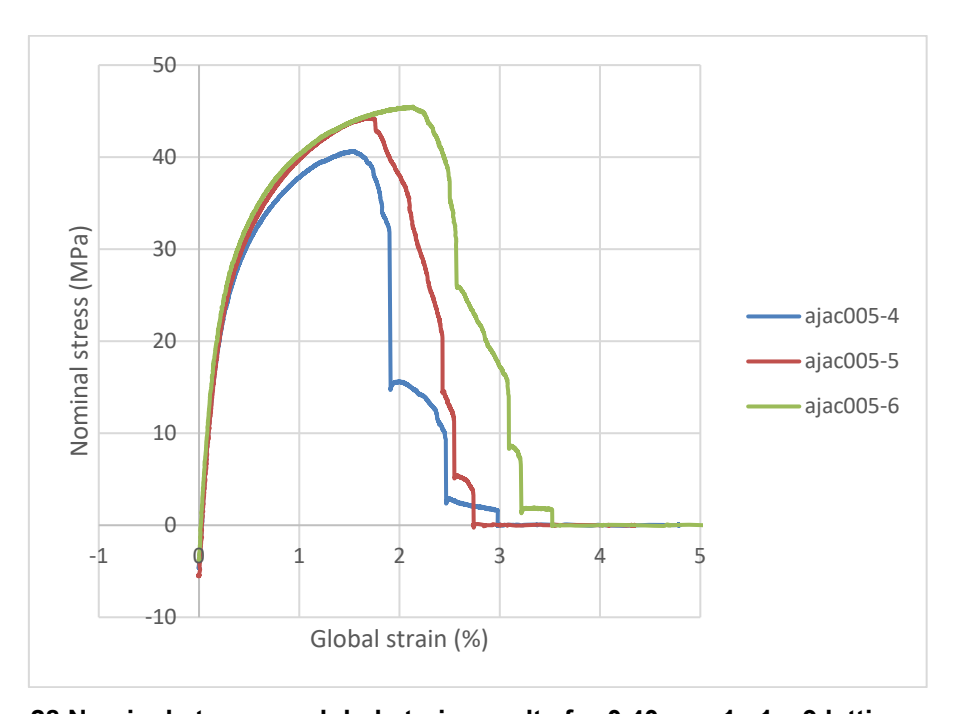


Figure 28 Nominal stress vs global strain results for 0.40 mm 1 x1 x 9 lattice samples

Figure 29 shows two images of failed 2 x 1 x 9 lattices, once again we observe the failure to be located in the central region, demonstrating how the design facilitates the use of non-contact strain measurement approaches. The load-displacement and nominal stress-global strain plots are shown in Figure 30 and Figure 31. With the increase in loading cross section we see an increase in the maximum load achieved, rising from \sim 36N to \sim 68N, but the nominal stress peaking around the same maximum value. The strain to failure is once again \sim 3%.

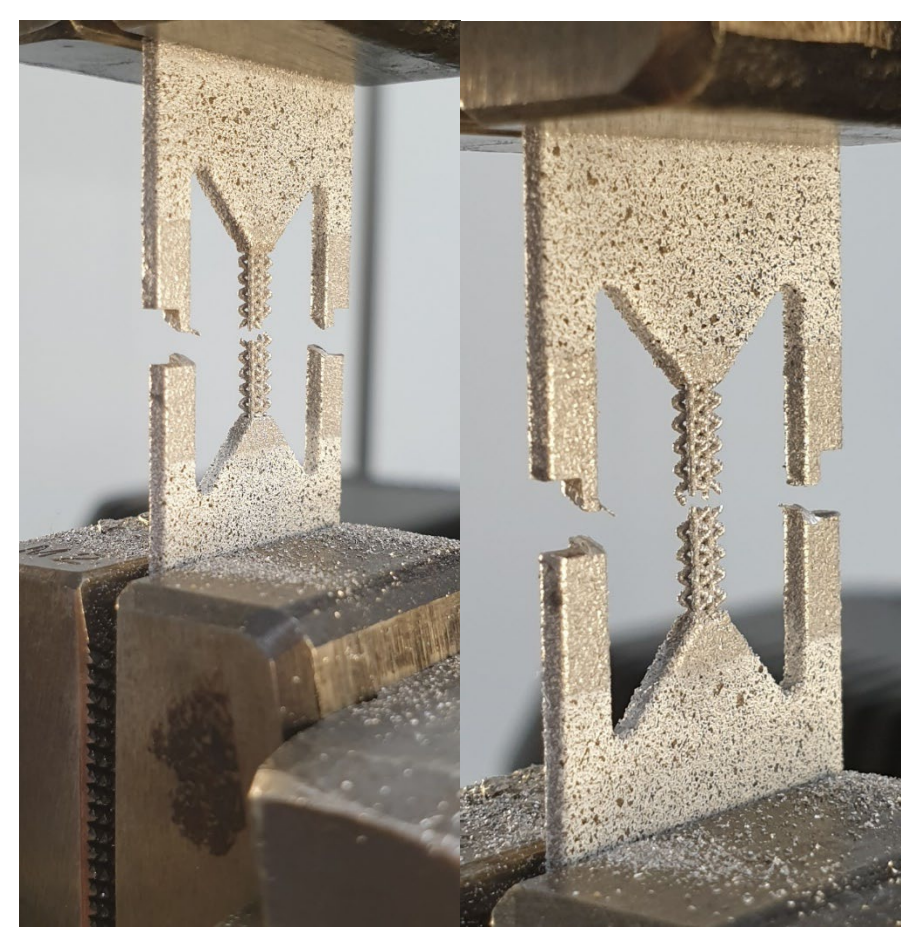


Figure 29 0.40 mm 2 x 1 x 9 lattice test pieces after testing

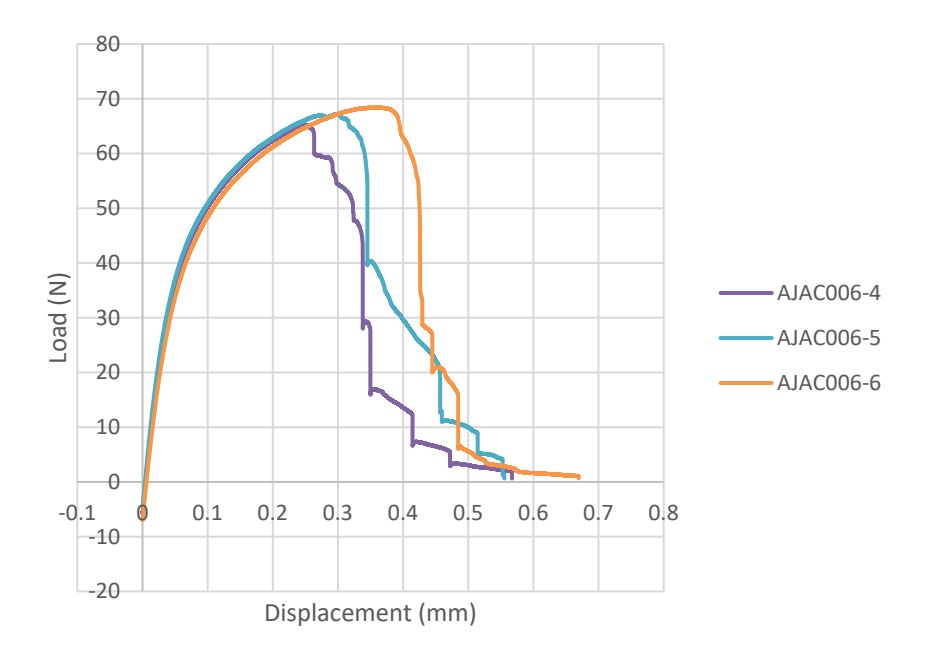


Figure 30 Load vs displacement results for 0.40 mm 2 x1 x 9 lattice samples

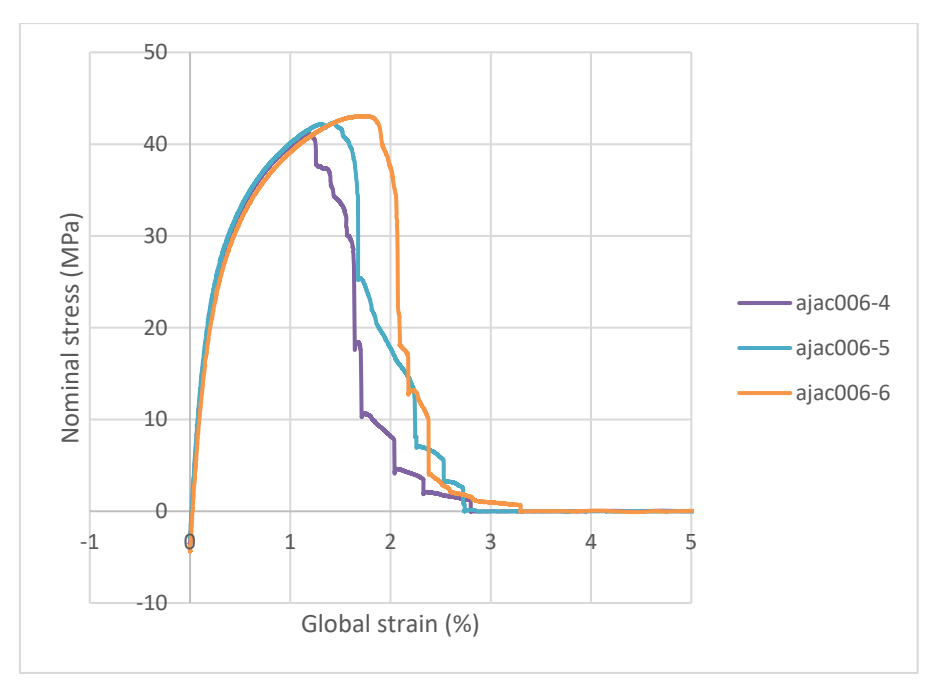


Figure 31 Nominal stress vs global strain results for 0.40 mm 2 x 1 x 9 lattice samples

Figure 32 shows two images of failed 5 x 1 x 9 lattices, as with previous sample configurations we observe the failure to be located in the central region. The load-displacement and nominal stress-global strain plots are shown in Figure 33 and Figure 34. With the increase in loading cross section we see an increase in the maximum load achieved, rising from \sim 36N to \sim 182N, and stress reaching a similar maximum vales as with the previous samples. The strain to failure is a little lower being around \sim 2%.

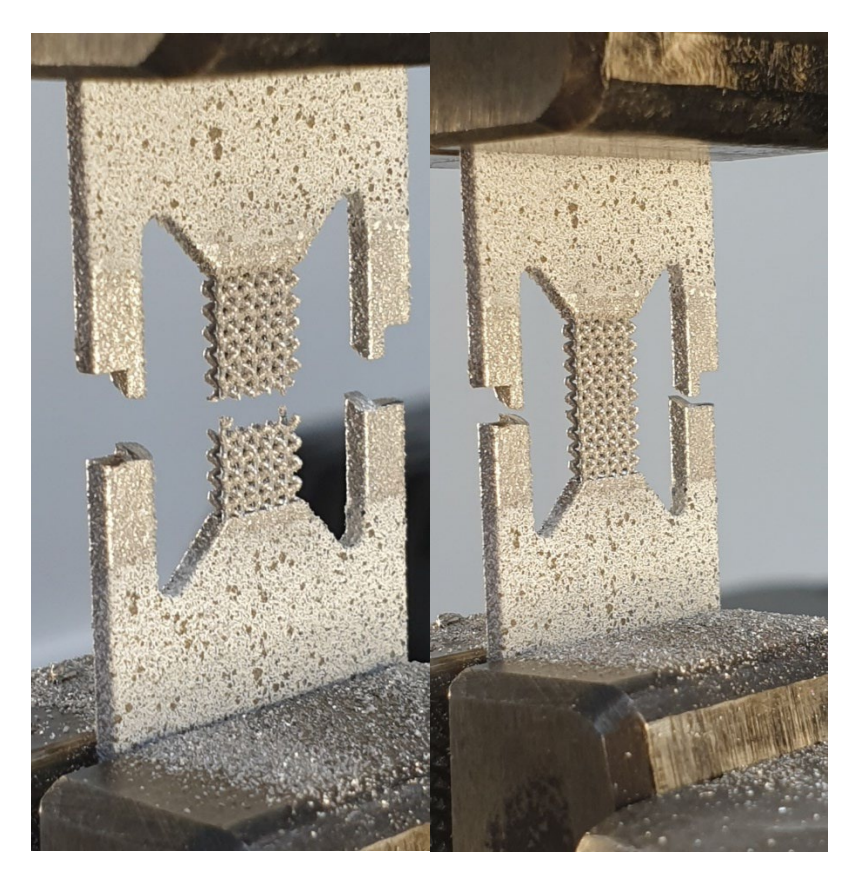


Figure 32 0.40 mm 5 x 1 x 9 lattice test pieces after testing

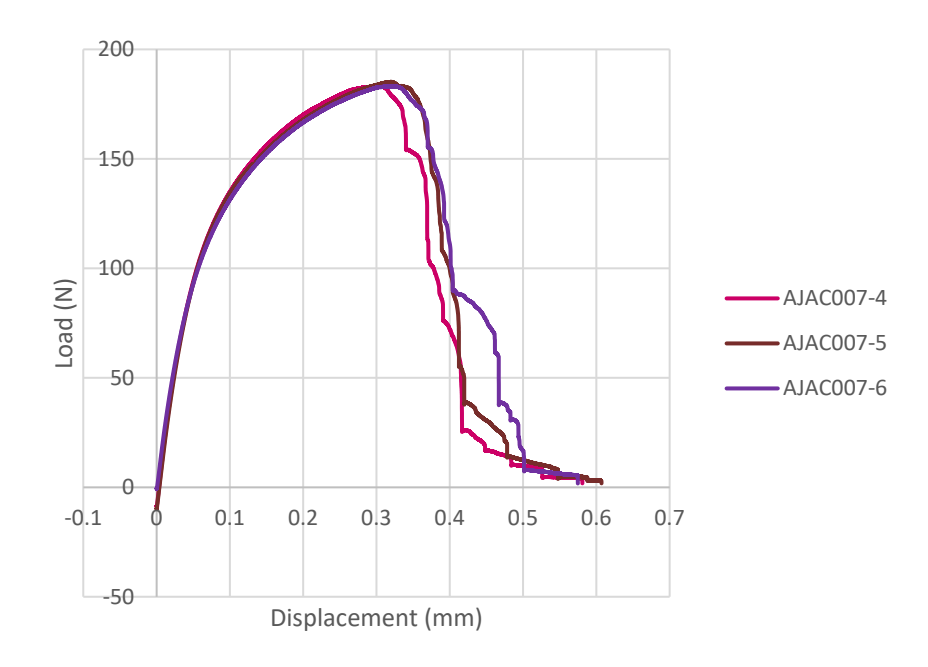


Figure 33 Load vs displacement results for 0.40 mm 5 x1 x 9 lattice samples

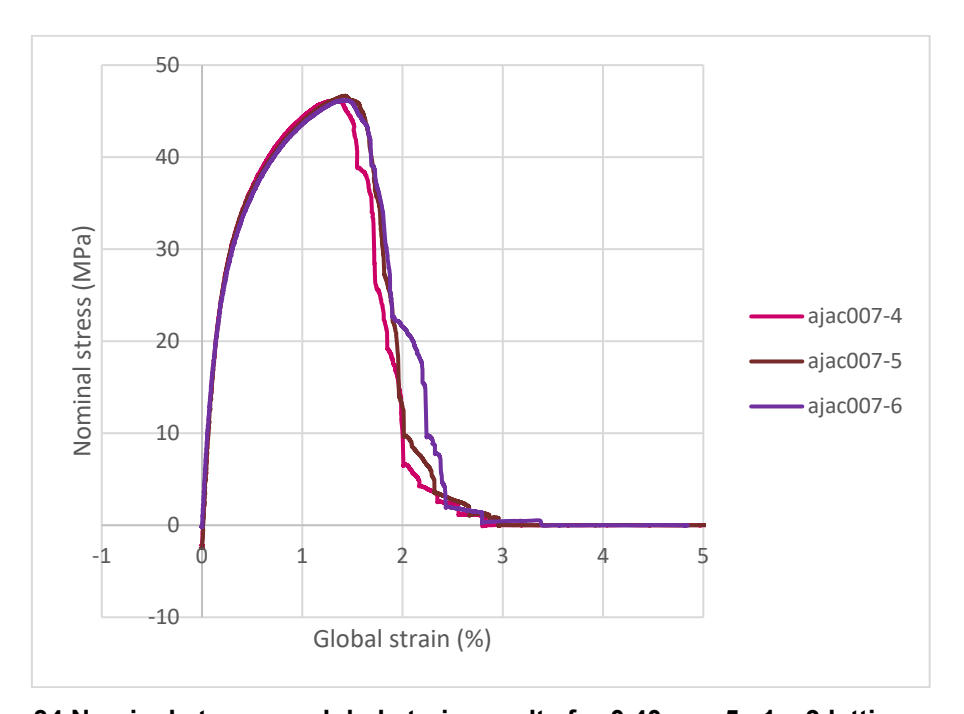


Figure 34 Nominal stress vs global strain results for 0.40 mm 5 x1 x 9 lattice samples

A comparison of the load and nominal stress plots for all geometries can be seen in Figure 35 and Figure 36 and the relationship between the maximum load achieved during testing as a function of number of unit cells in the sample cross section is given in Figure 37. This figure show that, gratifyingly, there is a linear relationship between the maximum load achieved during the test and the number of load bearing cells in the samples. This is as would be expected and demonstrates that the testing approach adopted is valid and robust, and that the actual quality of the AM build is good.

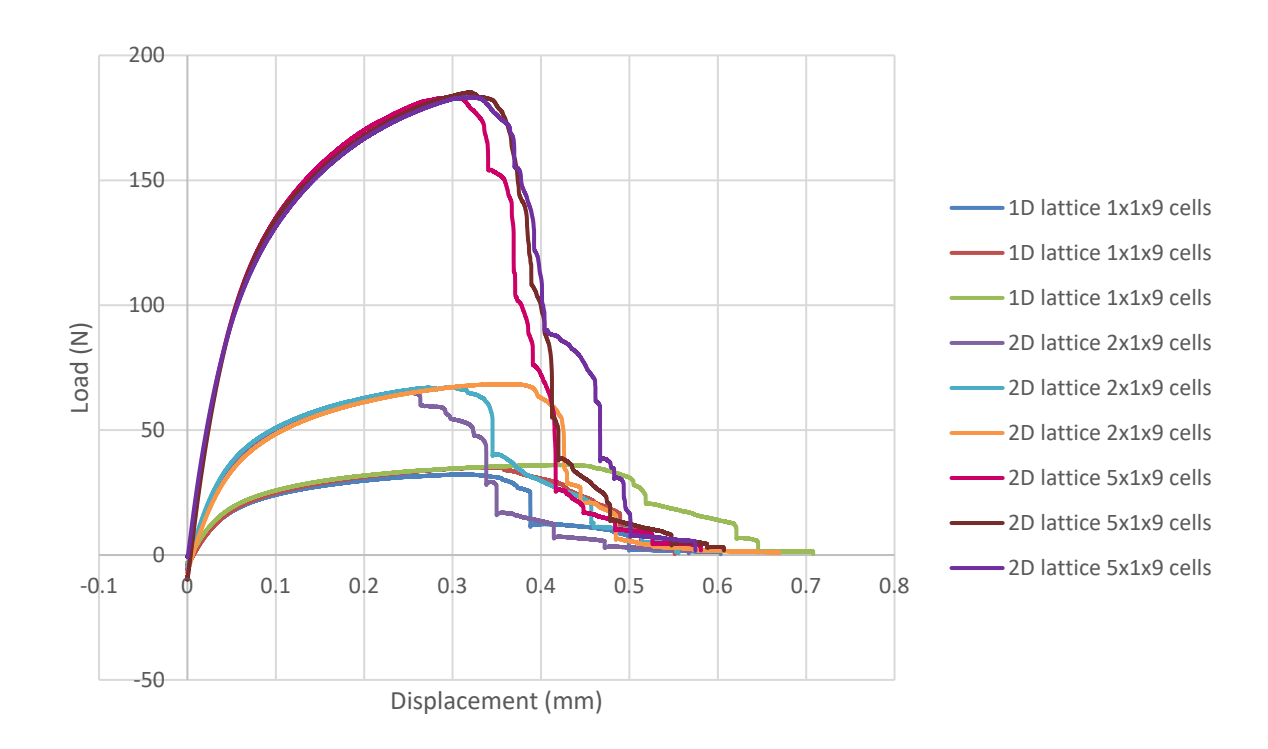


Figure 35 Comparison of load vs displacement results for the 0.40 mm lattice samples

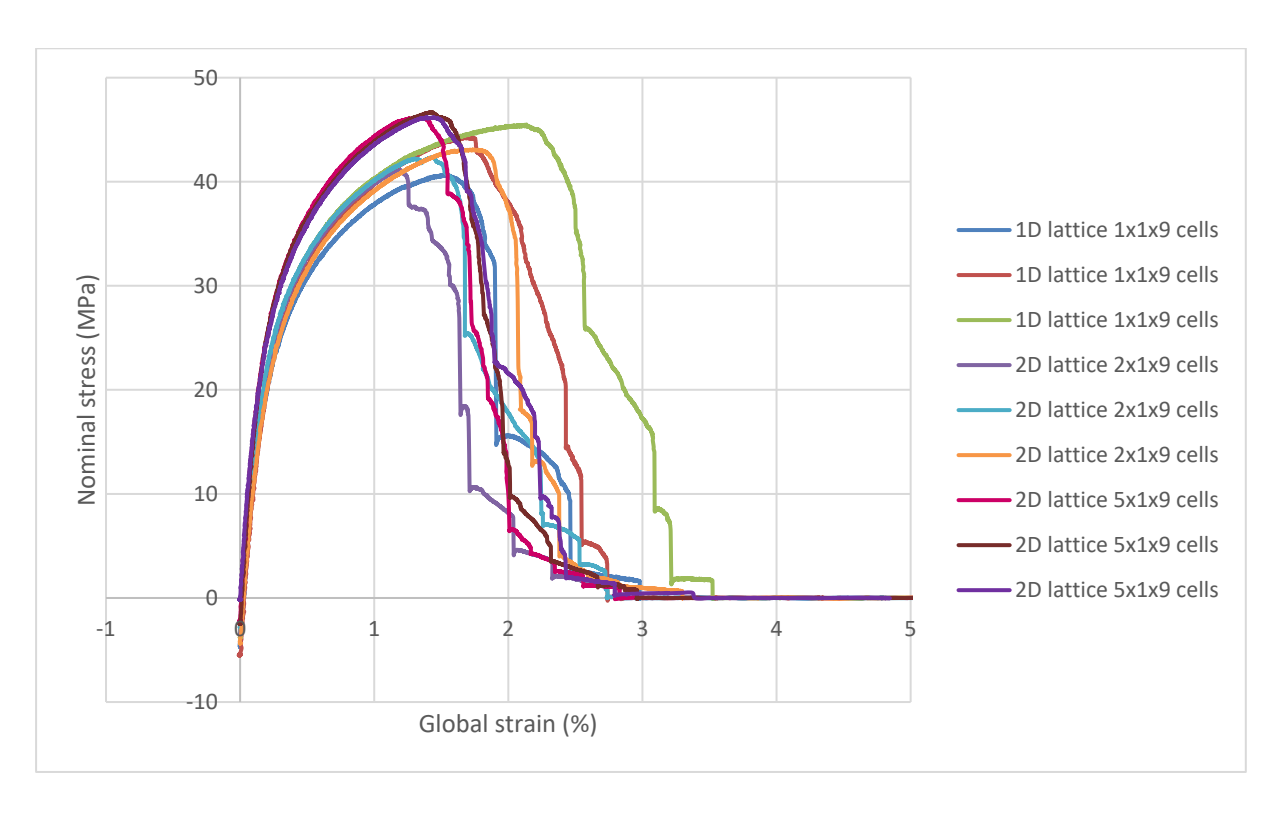


Figure 36 Comparison of the nominal stress vs global strain results for the 0.40 mm lattice samples

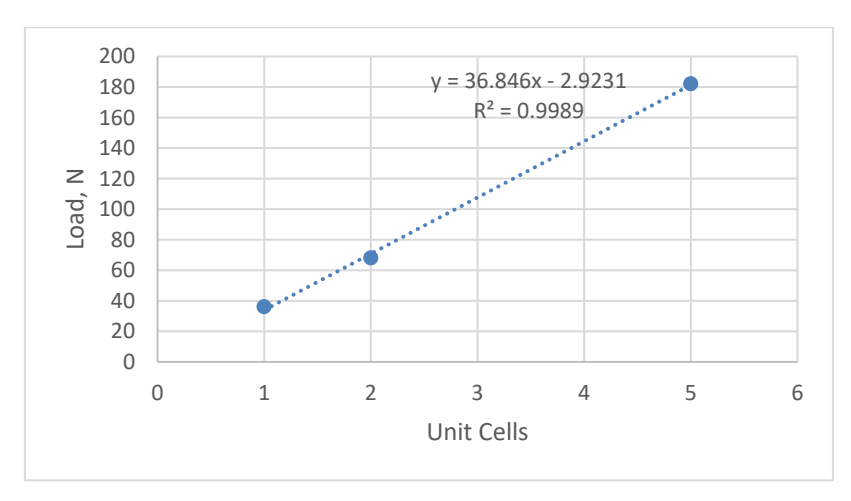


Figure 37 Relationship between load as a function of unit cells in the load bearing cross section

3.2 MICROMECHANICAL TESTING

The samples tested were single $0.5 \, \text{mm}$ and $0.75 \, \text{mm}$ diameter single ligament samples, and 1, 2 and 5 nodes samples with a $0.5 \, \text{mm}$ effective single unit cell diameter. The effective single unit-cell (or node) diameter was measured at the centre of Figure 38b. To allow for the mechanical testing to be conducted inside of the scanning electron microscopy (SEM), the specimen (Figure 38a) was further machines to remove the side supports, shorten the length of the sample to 22mm. Two 3.25 mm diameter holes were drilled at each end of the test specimen to allow the sample (Figure 38d) to be fitted onto the Deben MT2000EH rig to perform mechanical testing at room temperatures inside the Thermo Fisher Apreo scanning electron microscope (SEM), as shown in Figure 39. The SEM images showed that there were surface asperities on the gauge length. Measured optically, the minimum diameter was found to vary by less than 70 μ m.

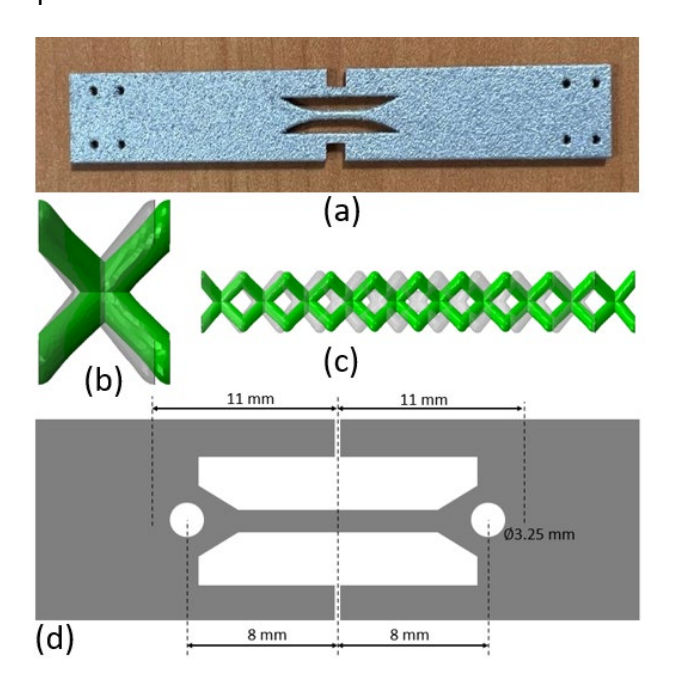


Figure 38(a) As received single ligament test specimen manufactured from AlSi10Mg. (b-c) Schematic of a single unit cell. (d) Schematic for a single ligament of the sample after it was machined

The tensile tests were conducted using a single leadscrew Deben MT2000EH test rig. This rig is a tensile, compression and horizontal bending stage designed for real-time observation of high-stress regions of a sample with an SEM, optical microscope, AFM, or XRD system. It uses custom miniature 2kN load cells. Samples are mounted horizontally, clamped to a pair of jaws, and supported on stainless steel slide bearings before being tested in tension.

To ensure accurate measurements, the 2 kN load cell was calibrated by the supplier. The test pieces were gripped using a pair of 3.25-diameter rods (Figure 39b).

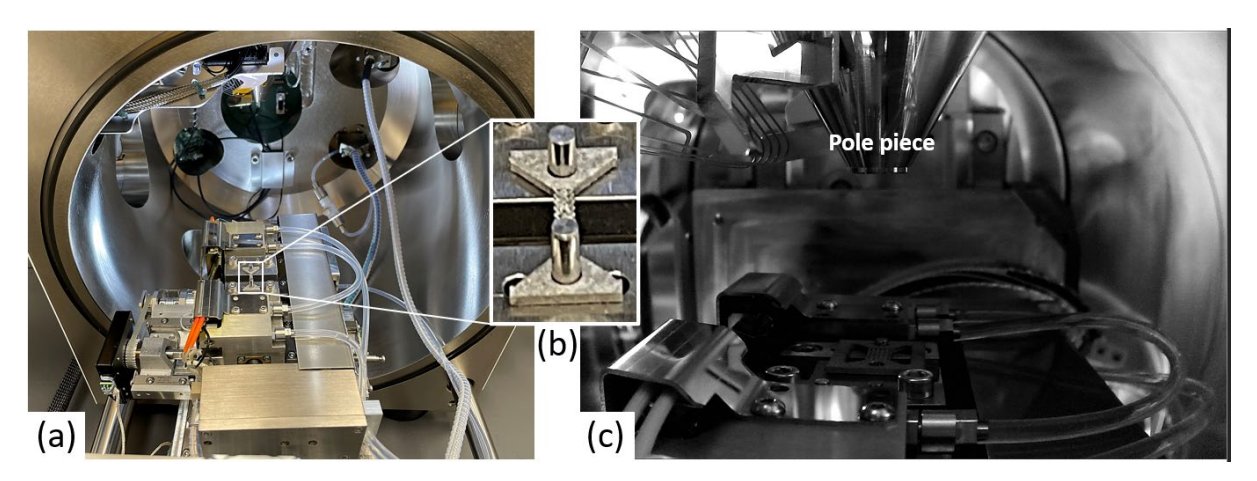


Figure 39(a) Deben MT2000EH rig after being fitted to the Thermo Fisher Apreo SEM's sample holder. (b) A close-up of a single unit cell sample fixed on the rig by 3.25 mm diameter rods. (c) The Deben rig inside the SEM is under vacuum at room temperature, with the sample being observed using secondary electrons

The test pieces were loaded at a crosshead speed of 0.1 or 0.2 mm per minute and deformed in tension. This speed is set to ensure a consistent extension rate during the test, which is essential for achieving accurate and consistent results.

The sample was imaged using the secondary electron (SE) at 10 kV and 1 nA beam conditions during testing. Non-contact strain measurement solutions were used to capture accurate and comprehensive data. They use imaging technologies and measurement techniques to accurately calculate multi-axis displacements, strains, and strain rates for any given test article. During testing, the sample was imaged inside the SEM to allow for non-contact strain measurement. The user can use a full field approach and measure the strain over the whole gauge length, or multiple discrete areas can be selected, allowing the user to simulate a standard strain gauge measurement, or markers combined with an image correlation extensometer approach can be employed.

The results of the in situ measurements performed on the three different lattice samples (1 x 1 x 9, 2 x 1 x 9 and 5 x 1 x 9) are presented in Figure 40 which shows the Deben data. Figure 41 compares this Deben data with that collected using the Instron Universal Test system.

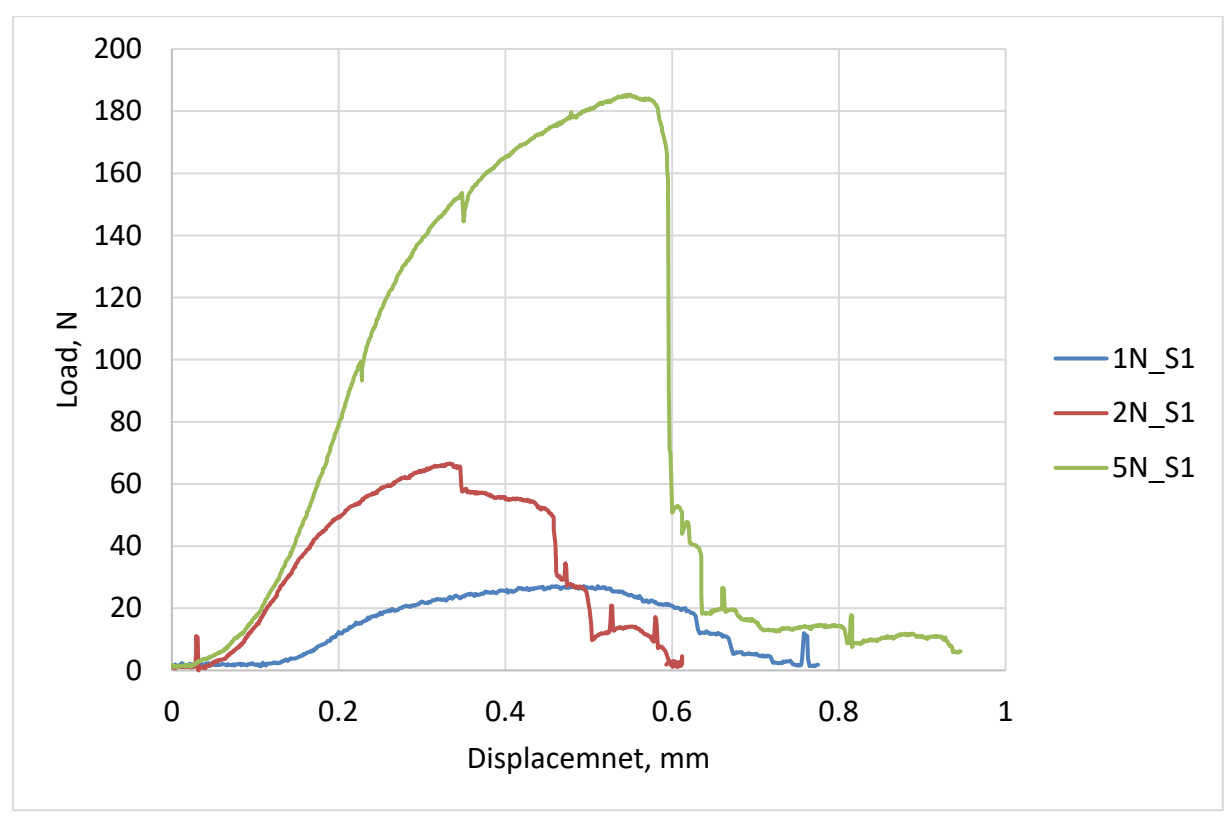


Figure 40 Load vs displacement plot for the 3 lattice structures (1 x 1 x 9, 2 x 1 x 9 and 5 x 1 x 9) tested in the Deben test stage

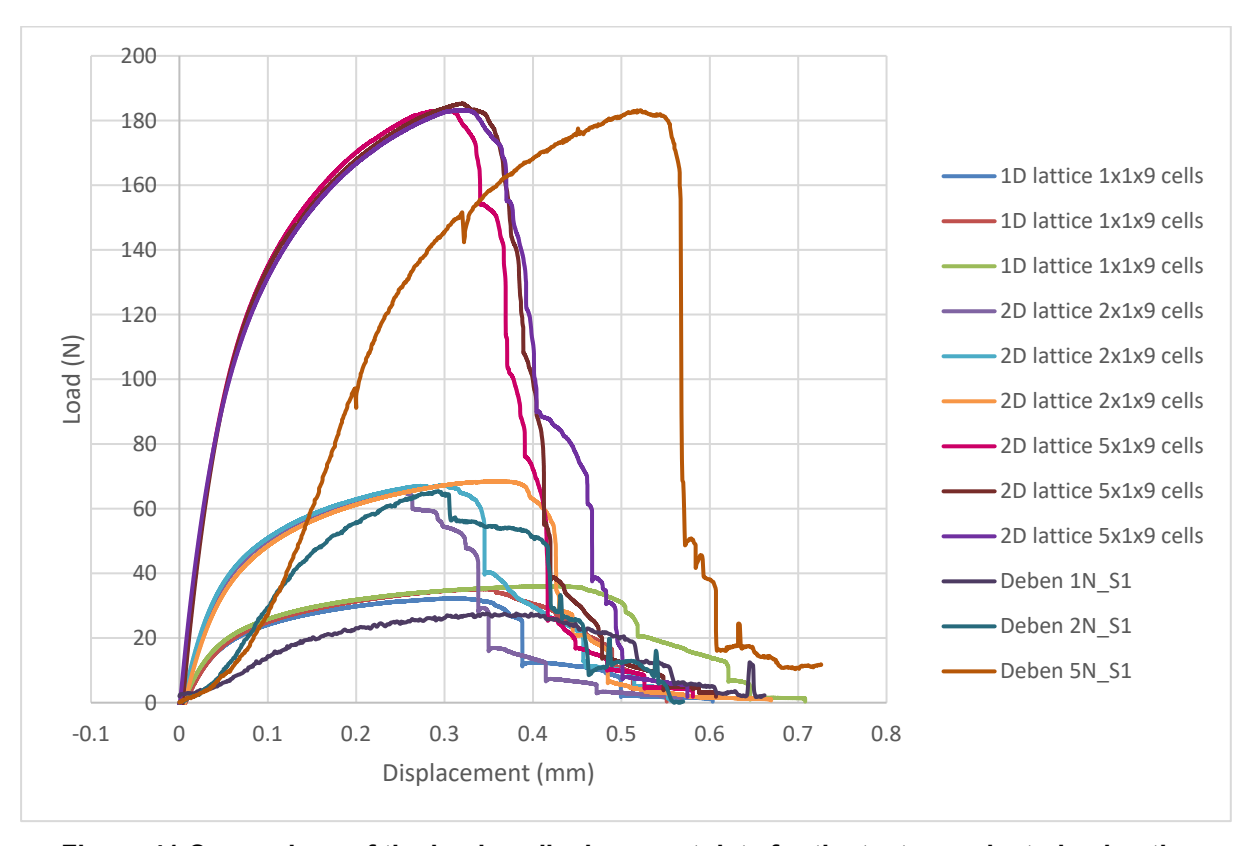


Figure 41 Comparison of the load vs displacement data for the tests conducted using the Deben and Instron test frames

Comparing the data from the in situ Deben test rig with the Instron UTS data, it can be seen that the maximum loads reached agree very well across the three different specimen types with a near 1:1 correlation (Figure 42). The actual load displacement comparison shows that there are some differences in the rig compliance which may resolve itself when considering stress and strain plots, not considered here. Figure 43 shows the load vs displacement curves for the samples tested. Points 1 and 2 show a drop in load, this was where the test was paused for image capture. Points 3, 4 and 5 show where the ligaments failed sequentially on the test piece as is the case with points 6 and 7. This sequential failure was also observed in the Instron data.

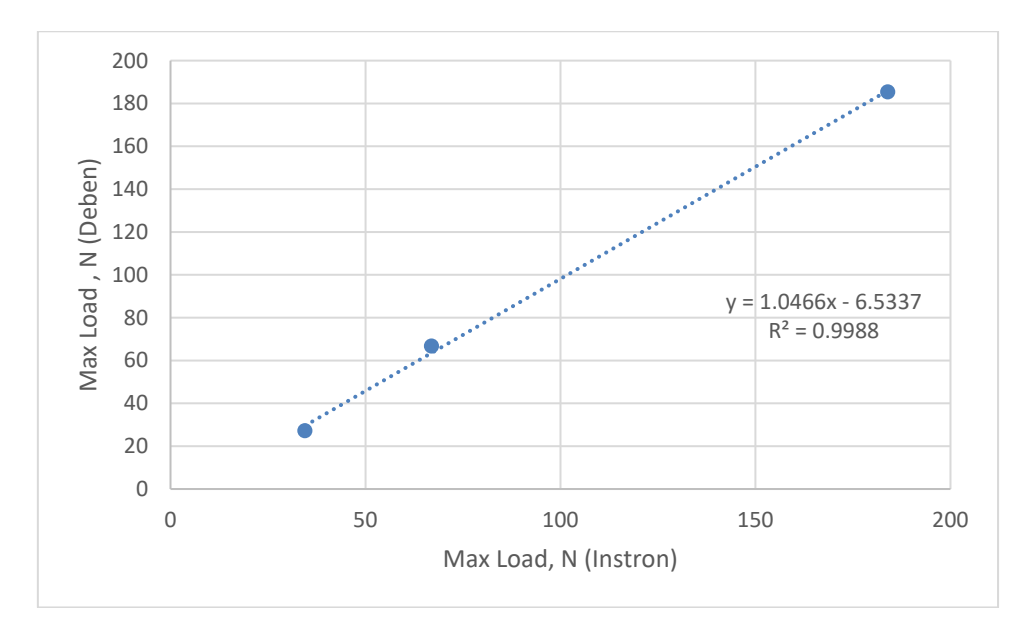


Figure 42 Comparison of maximum loads achieved in the Deben and Instron tensile tests

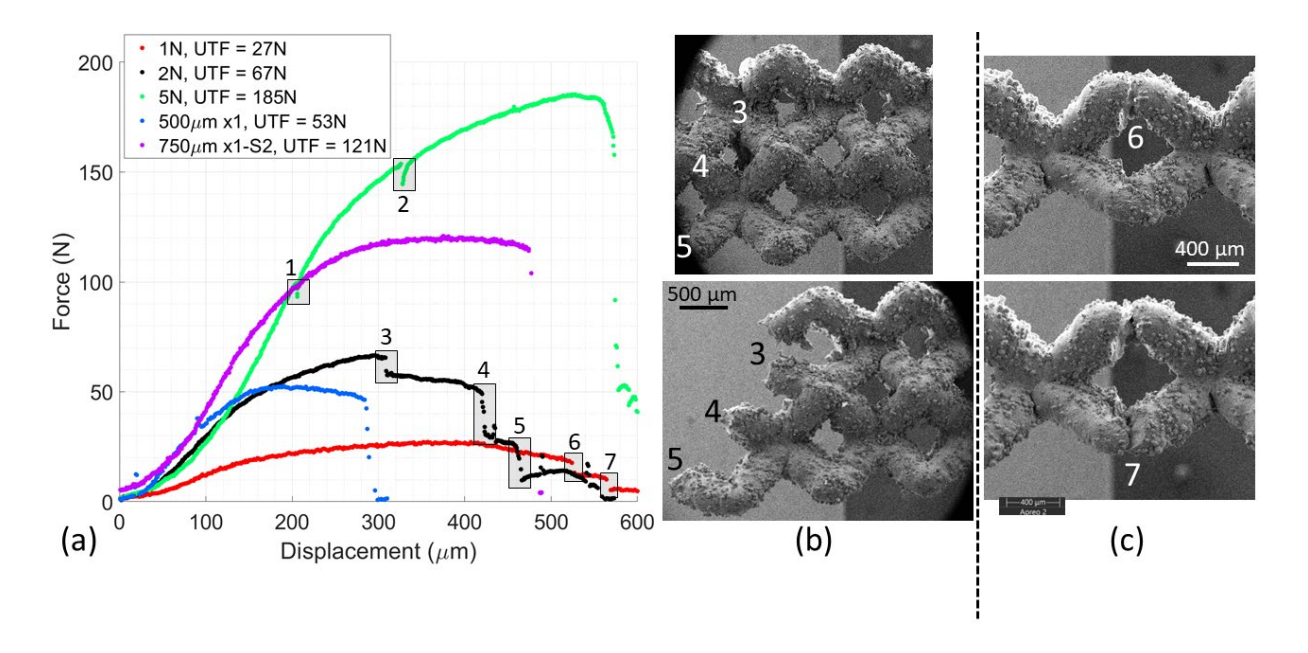


Figure 43 Load vs displacement plots and micrographs for micromechanical tests conducted on the lattice structures

3.3 NANOMECHANICAL TESTING

To examine the variability in the mechanical properties within the lattice structure a series of nanomechanical tests were conducted using an instrumented nanoindenter. The Nano Test Xtreme nanoindentation system, shown in Figure 44 was used for these measurements. The test system benefits form a high spatial resolution (\sim 1 nm) coupled with high depth resolution (\sim 0.1 nm) to be able to conduct nanoindentation tests over a load range of 1 μ N to 0.5 N.



Figure 44 Nano Test Xtreme nanonindentation test system

Initial measurement were made on the single ligament sample in three locations, in two areas in the centre of the gauge length (map 1 and 3) and one area to the end of the ligament (map 2) as shown in Figure 45. These maps were made on the 0.3 mm diameter ligament with a maximum load of 4 mN with a pitch of 4 μ m, total of 576 indents per map. The indents were made with a diamond Berkovich indenter (Poisson's ratio of 0.07, Young's modulus of 1141 GPa) which had been calibrated against fused silica for area function, the indentation results were analysed with AlMgSi10 Poisson's ratio of 0.3.

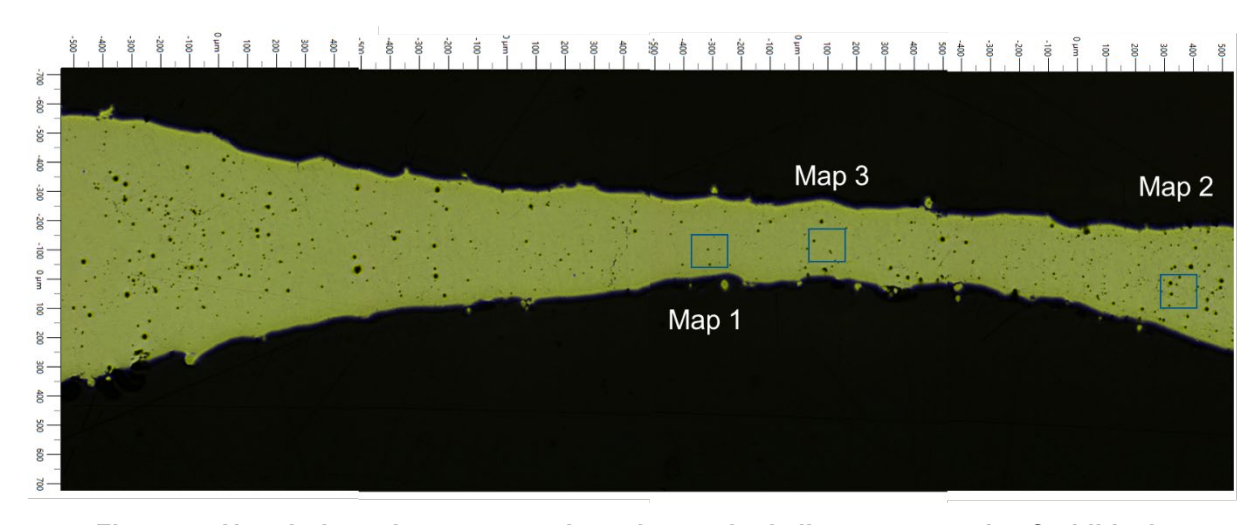


Figure 45 Nanoindentation tests conducted on a single ligament sample of additively manufactured AlSi10Mg

The results for these three maps are shown in Figure 46, this shows the hardness and elastic modulus to be uniform where there is less pores observed from the surface. The results of map 2 are more scattered, with slightly lower Young's modulus and hardness values, which could be attributed to porosity. The results of Young's modulus values of different maps are summarised in Table 2.

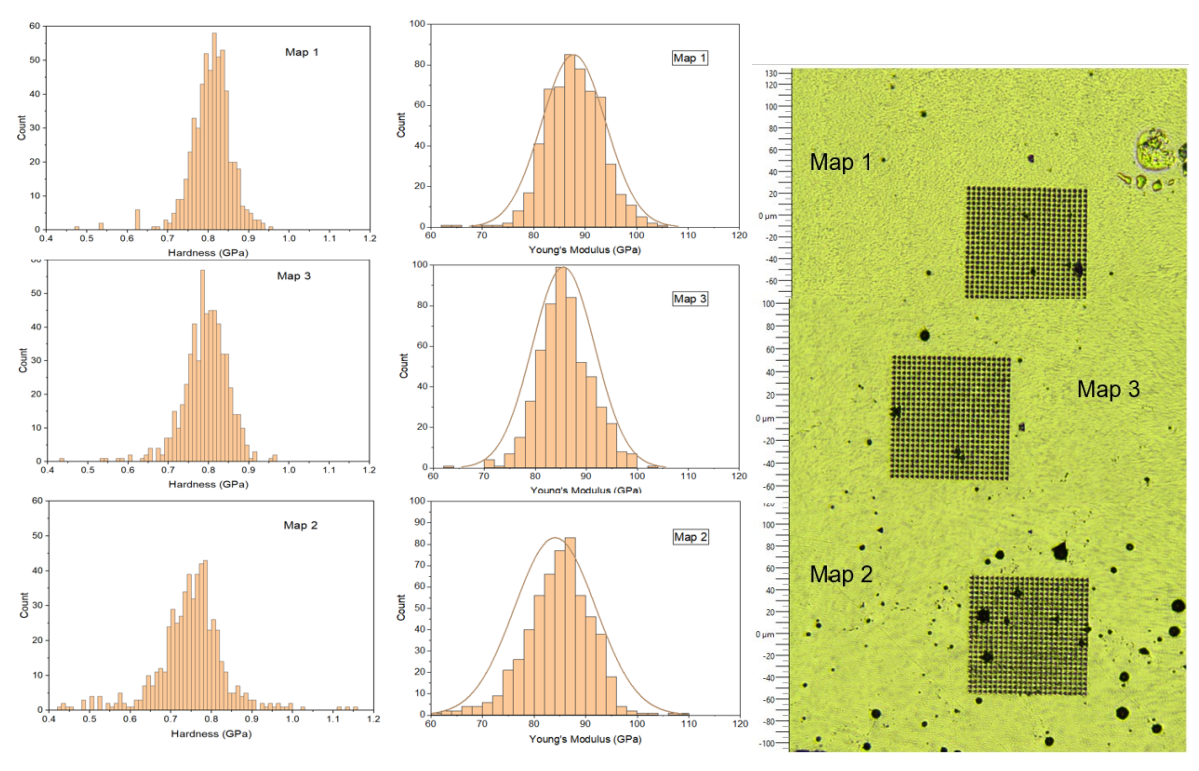


Figure 46 Hardness and elastic modulus histograms and indent maps for the three areas tested on the single ligament sample

In addition to these measurements a series of indents was made on the as manufactured lattice unit cells. This required the sample to be mounted and carefully sectioned and polished to reveal the areas of interest. These were within the arm structure (at the edge and in the centre) shown in Figure 47 together with the nanoindentation mapping results, and within the node, shown in Figure 48 with results shown in two selected regions.

The results from the edge of the arm (map 1) shows similar mechanical properties to the single ligament. Despite a lower hardness in the middle of the arm structure (map 2) compared to the edge, the Young's modulus is about 5% lower. After a closer examination, the edge of the arm (map 1) has nearly no pores, while the middle section (map 2) shows apparent pores and fusion lines.

Furthermore, the tests in different regions of the node structure shows similar Young's modulus, except for map 3 which is lower. The lower Young's modulus could be caused by the effect of the resin (thinner sample compared with middle section of the arm where higher values were measured (map 4). Together with the single ligament results, the Young's modulus values of the lattice from different regions are presented in Table 2. In summary, Young's moduli were quite similar to those on the single ligament showing very little difference across the different regions examined. As a result of these measurements, it was concluded that in this case the properties, at least modulus, could be considered as uniform throughout the lattice where the effect of pores are excluded.

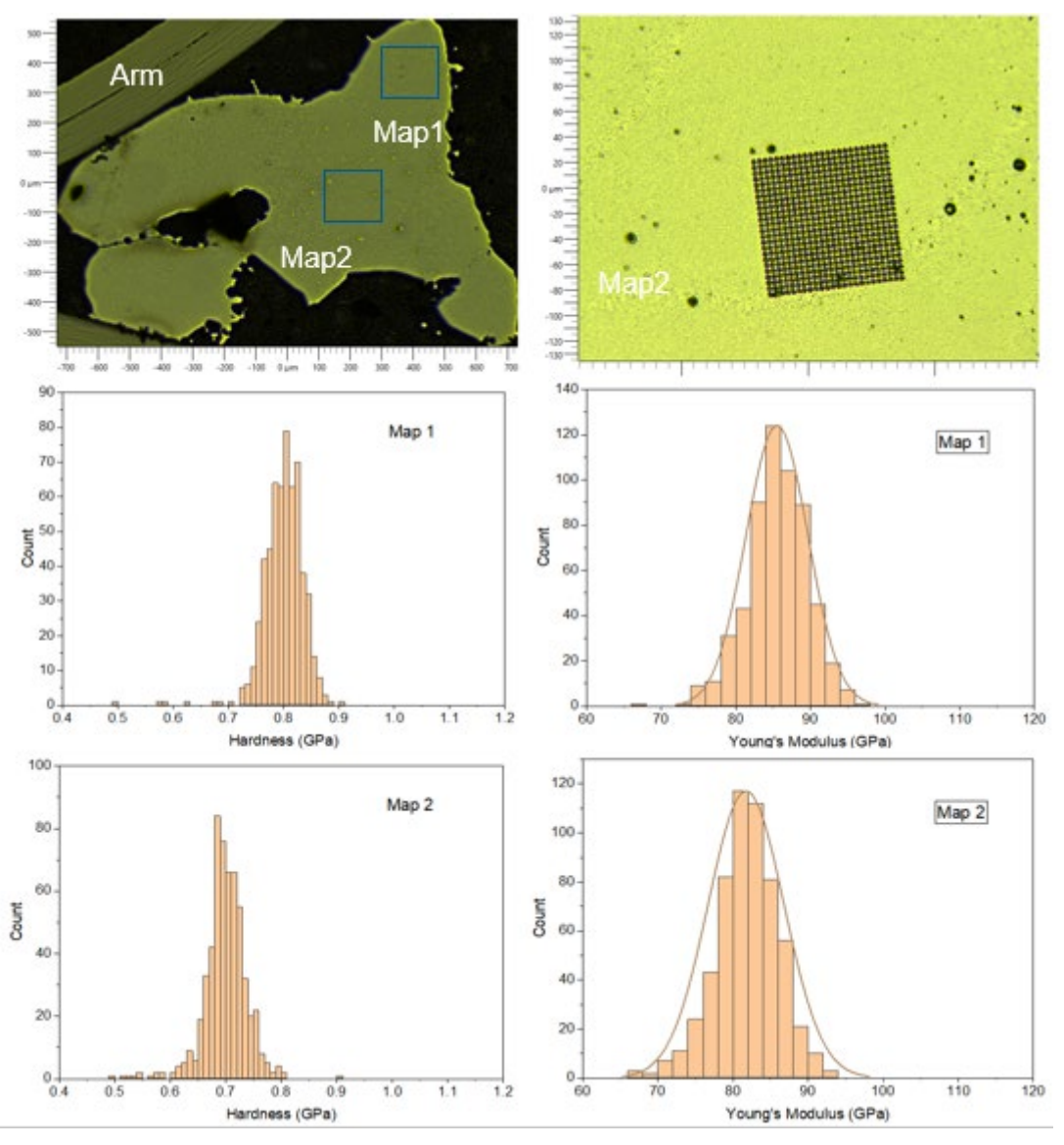


Figure 47 Areas of interest for nanoindentation measurement, details of the Map2, and histograms of hardness and elastic modulus values of two regions in the arm of the lattice cell

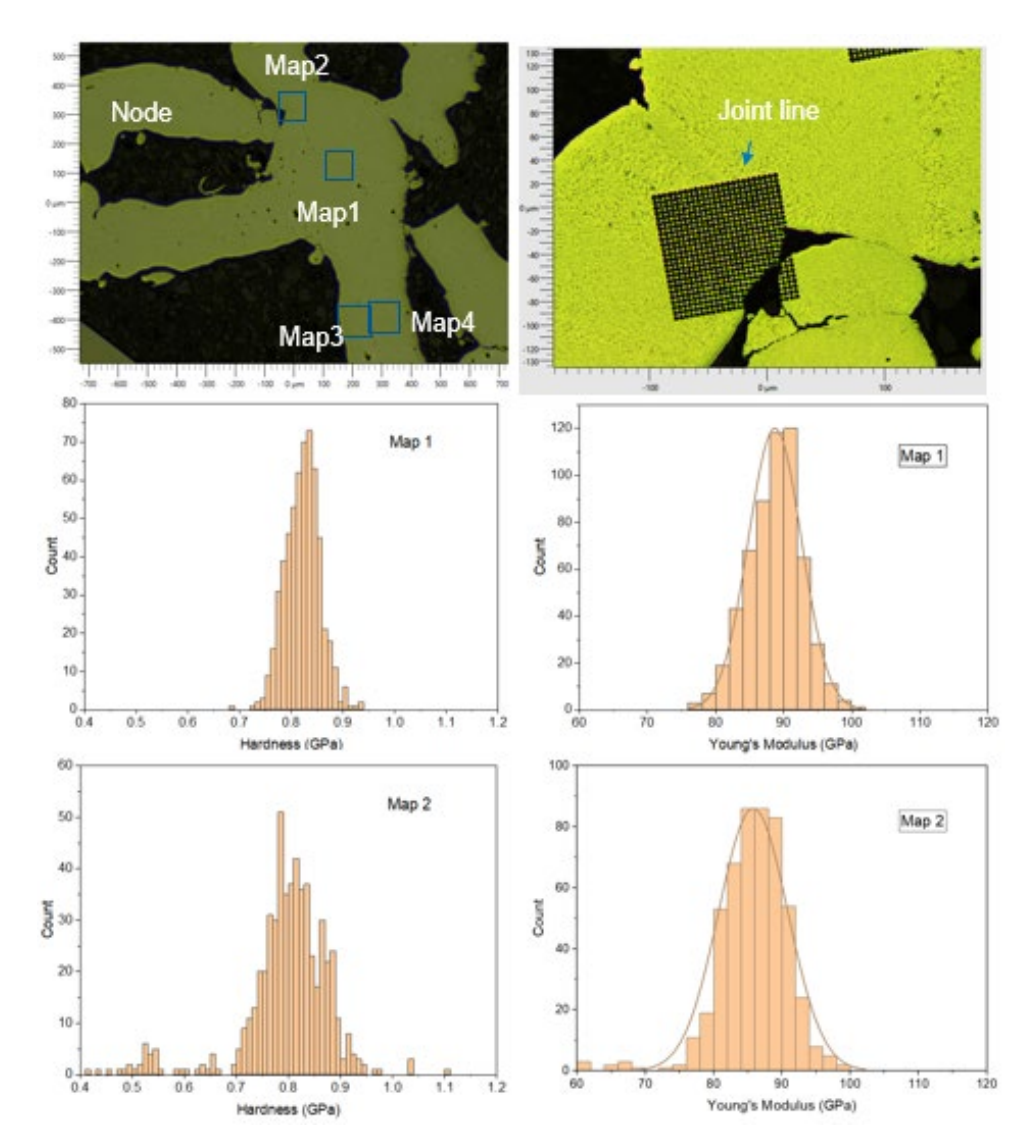


Figure 48 Areas of interest for nanoindentation measurement, details of Map2 and the histograms of the hardness and eleastic modulus values of two selected areas in the node of the lattice cell

Table 2 A summary of nanoindentation results on different regions

Sample	No of map	Mean (GPa)	Stdev (GPa)	Median (GPa)	No of indents
	Map 1	87.7	6.2	87.7	576
	Map 2	84.1	7.9	85	576
Ligament	Map 3	85.5	6.1	85.5	576
	Map 1	84.1	4.2	84.2	576
Lattice Arm	Map 2	80.1	5.0	80.3	576
	Map 1	87.5	3.9	87.7	576
	Map 2	84.4	5.1	84.8	511
	Map 3	77.6	85.6	78.6	402
Lattice Node	Map 4	81.1	4.0	81.2	522

4 FINITE ELEMENT MODELLING

4.1 SINGLE LIGAMENT MODEL

The finite element analysis (FEA) software package Abaqus was used to model the behaviour of a ligament sample with a cylindrical central section. Five models were created for different diameter specimens (d = 0.3, 0.4, 0.5, 0.75 and 1 mm) with the gauge length region being 4 x d in each case, see Figure 49.

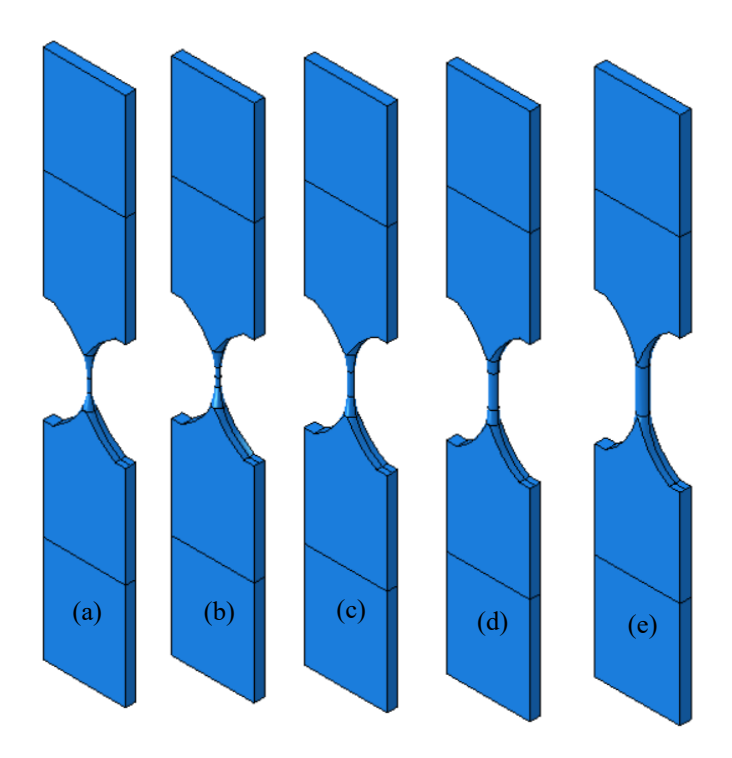


Figure 49 Final geometries for ligaments with diameters of (a) 0.3 mm, (b) 0.4 mm, (c) 0.5 mm, (d) 0.75 mm and (e) 1 mm

Grip regions were created, and the lower grip region was fully constrained. The top grip region was constrained in the x- and z-directions. All nodes in the top grip region were tied to a single node in the y-direction by an equation. This meant that the overall displacement could be applied to this single node, and this node could be used to output the total reaction force. These boundary conditions are shown in Figure 50(a). A displacement of 0.225 mm was applied to the 0.5 mm diameter geometry and 0.3 mm displacements were applied to the 0.7 mm and 1 mm diameter ligaments.

A fine mesh was created on the main section of the sample with a coarser mesh in the grip regions, see Figure 50(b), using quadratic tetrahedron, type C3D10 elements. A node set containing gauge nodes was also created, Figure 50(c), to enable strain calculation from the parallel sided region.

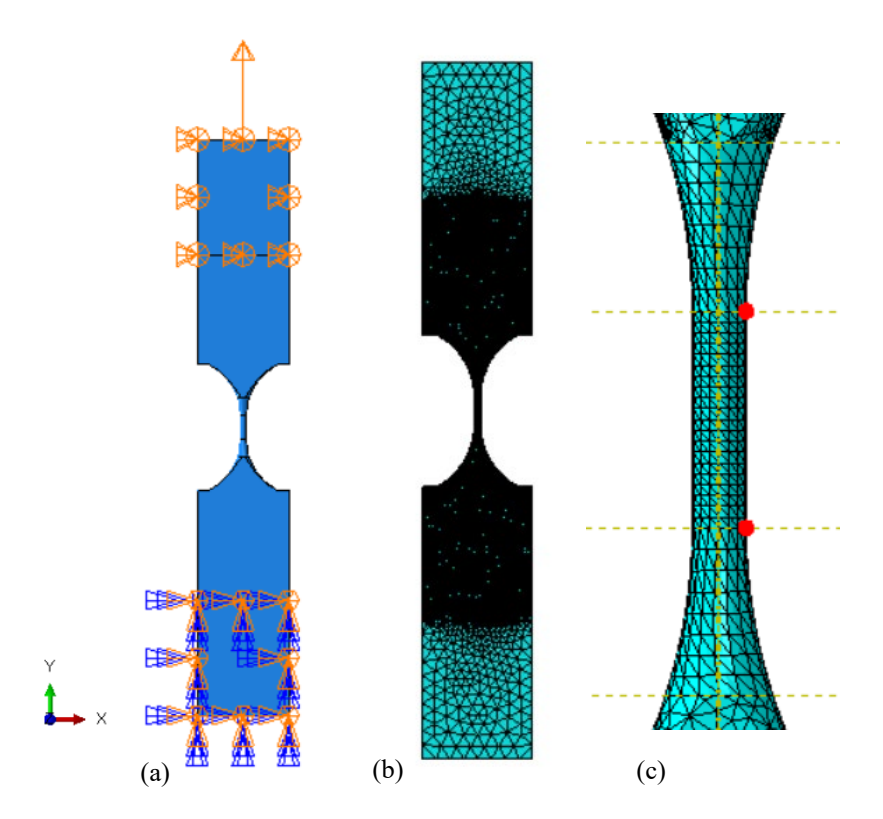


Figure 50 Ligament geometry showing (a) boundary constraints, (b) mesh and (c) location of gauge nodes

The material properties were obtained from the single ligament tests, see Figure 12, using data from the 1 mm diameter, 3 mm gauge length specimen. An elastic-plastic material model was used to represent the AlSi10Mg alloy, with a Young's Modulus of 67446 MPa and a Poisson's ratio of 0.33. Elastic-plastic models require a hardening curve of stress vs plastic strain to define the plastic behaviour of the material. The hardening curve obtained from the stress-strain data is shown in Figure 51.

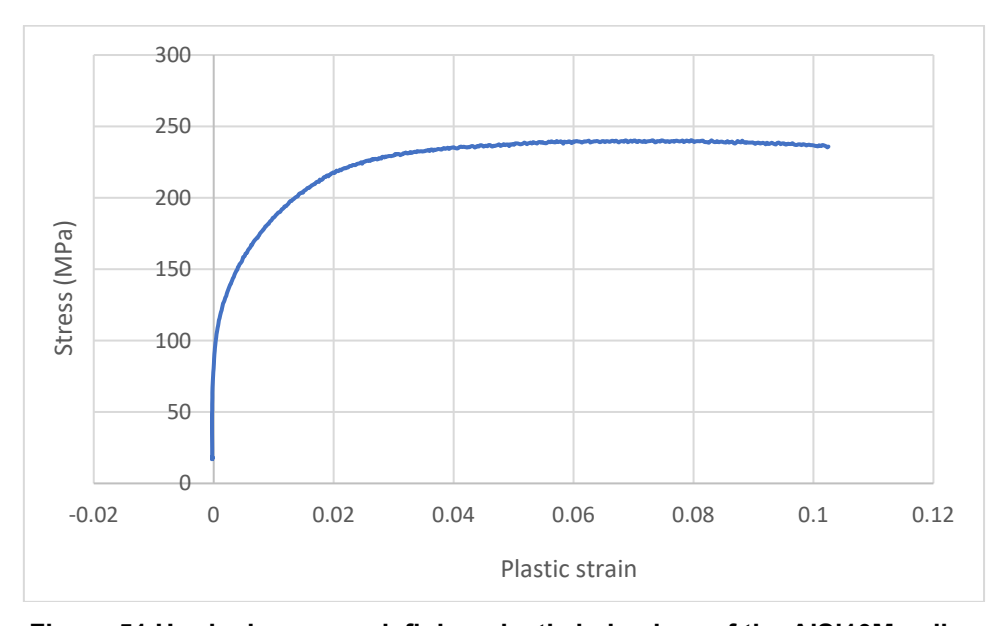


Figure 51 Hardening curve defining plastic behaviour of the AlSi10Mg alloy

The predicted load-displacement curves for the five geometries are shown in Figure 52. The predicted load-displacement curves for the 0.5 mm, 0.75 mm and 1 mm diameter ligaments are compared to the experimental data in Figure 53 and are found to correlate well.

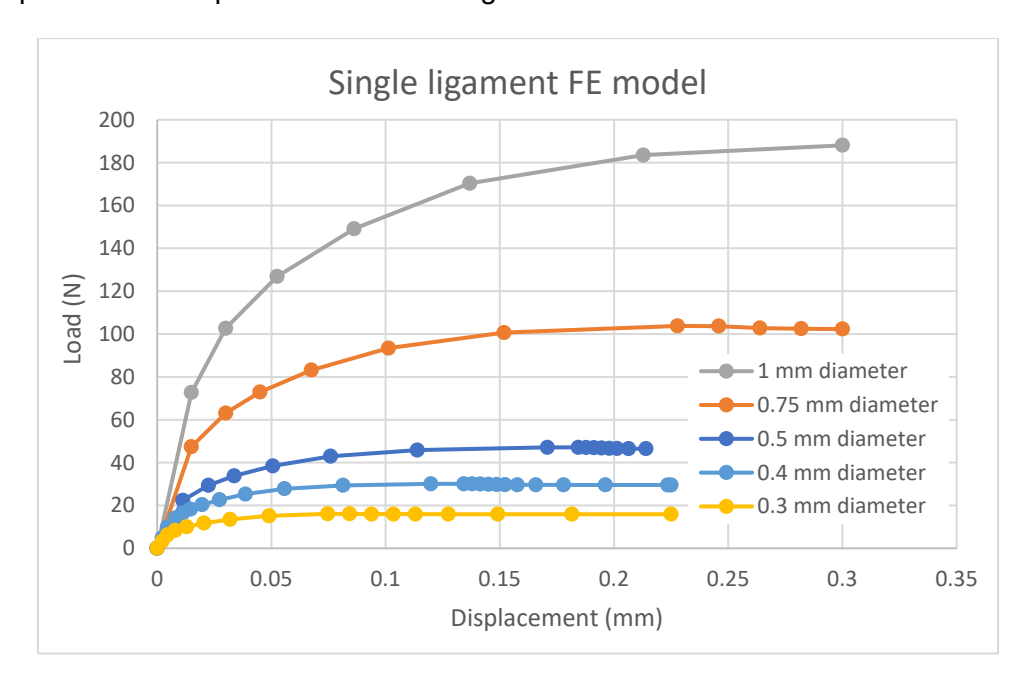


Figure 52 Predicted load-displacement plots for the five different diameter ligament models

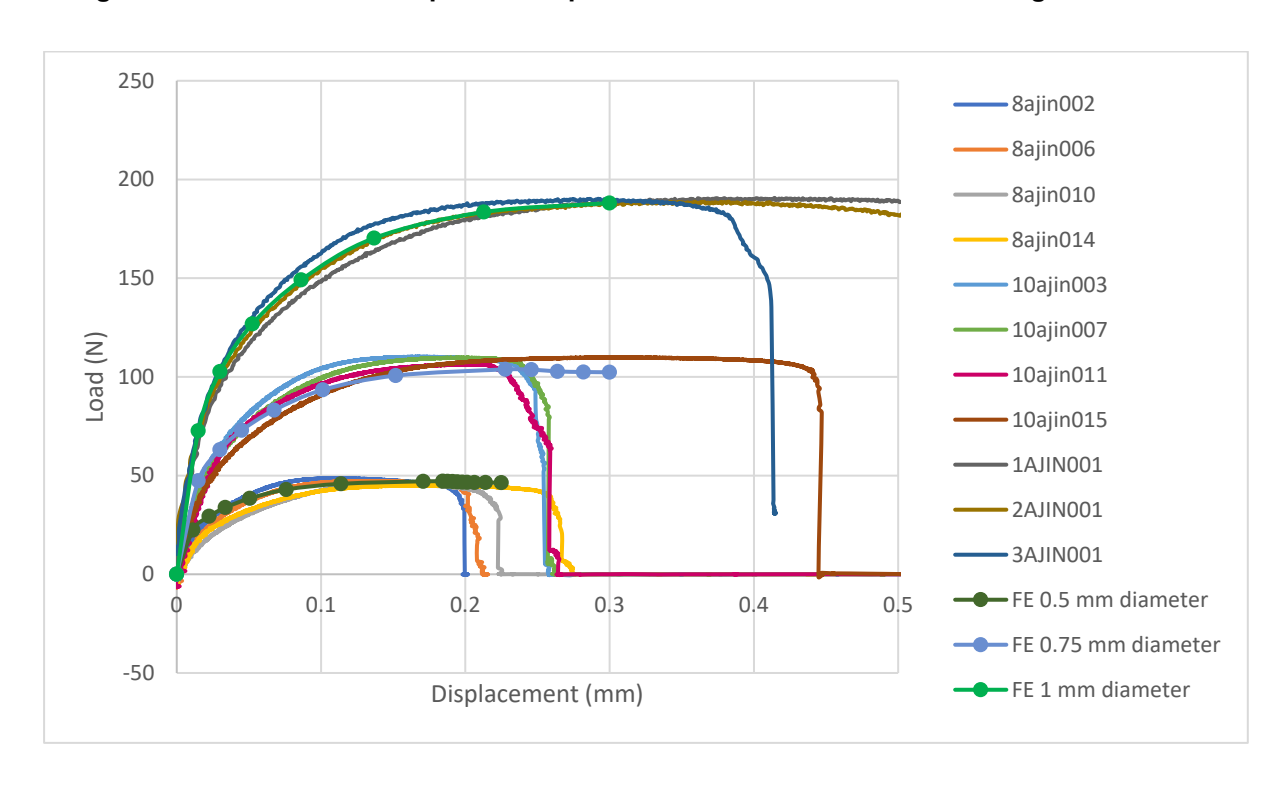


Figure 53 Comparison of FE predictions and experimental data for the 0.5 mm, 0.75 mm and 1 mm diameter ligament geometries

Figure 54 shows the predicted stress-strain plots for the five geometries. The stress-strain plots are consistent with each other and represent the material response described within the FE models material definition.

The predicted stress-strain response of the 1 mm diameter geometry has been compared to experimental data from 1 mm diameter specimens. The FE prediction correlates well with the measured behaviour, Figure 55.

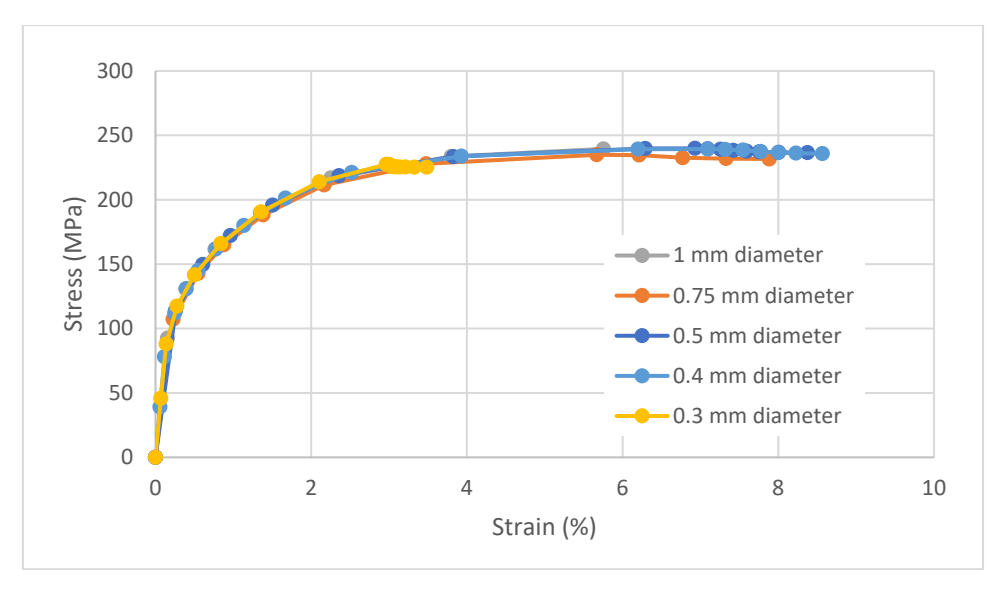


Figure 54 Predicted stress - strain plots for the five different diameter ligament models

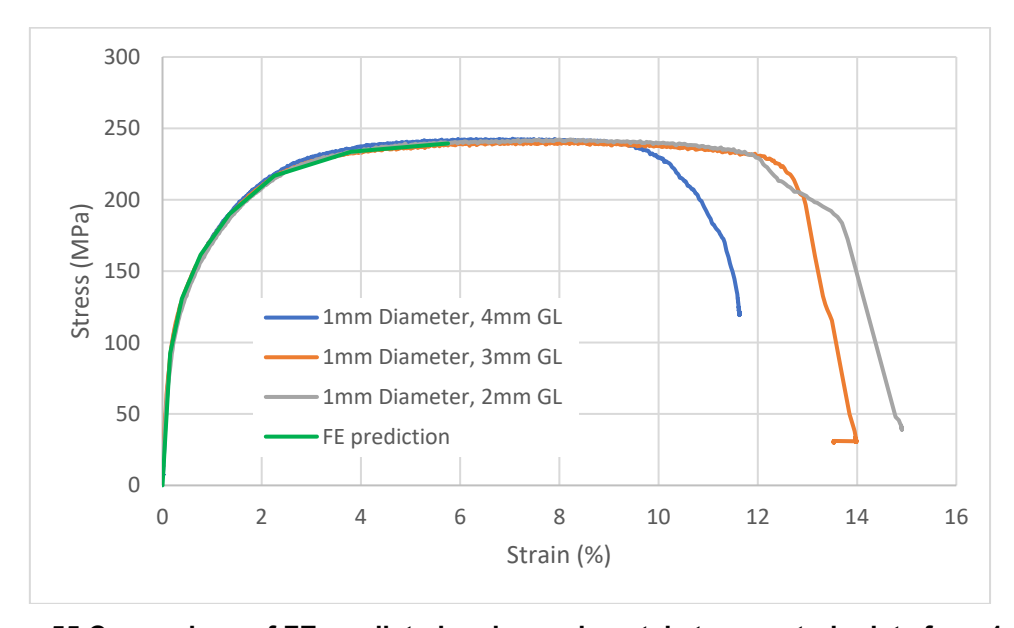


Figure 55 Comparison of FE predicted and experimental stress - strain data for a 1 mm diameter ligament specimen

The predicted maximum load has been plotted against ligament diameter. When results from the 0.5 mm, 0.75 mm and 1mm cases are plotted, the slope of the line is very similar to that obtained from the experimental data, see Figure 56, but when all diameters are included, the plot becomes less linear (Figure 57), suggesting that at smaller diameters, a ligament will sustain a higher load than expected from the linear fit.

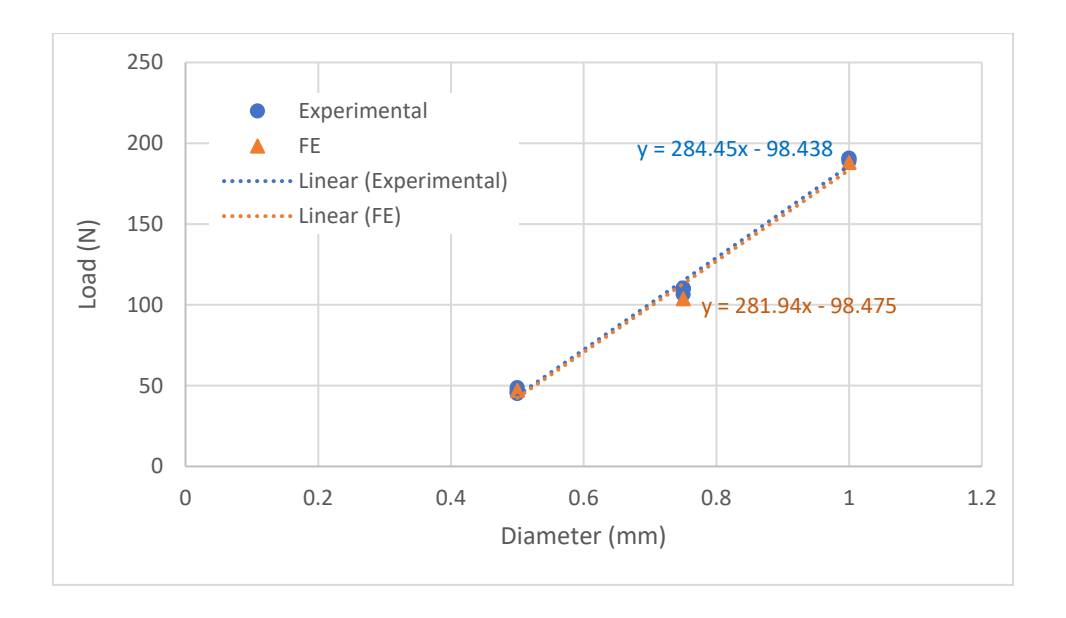


Figure 56 Comparison of experimental and FE maximum load versus ligament diameter for the larger three diameter geometries

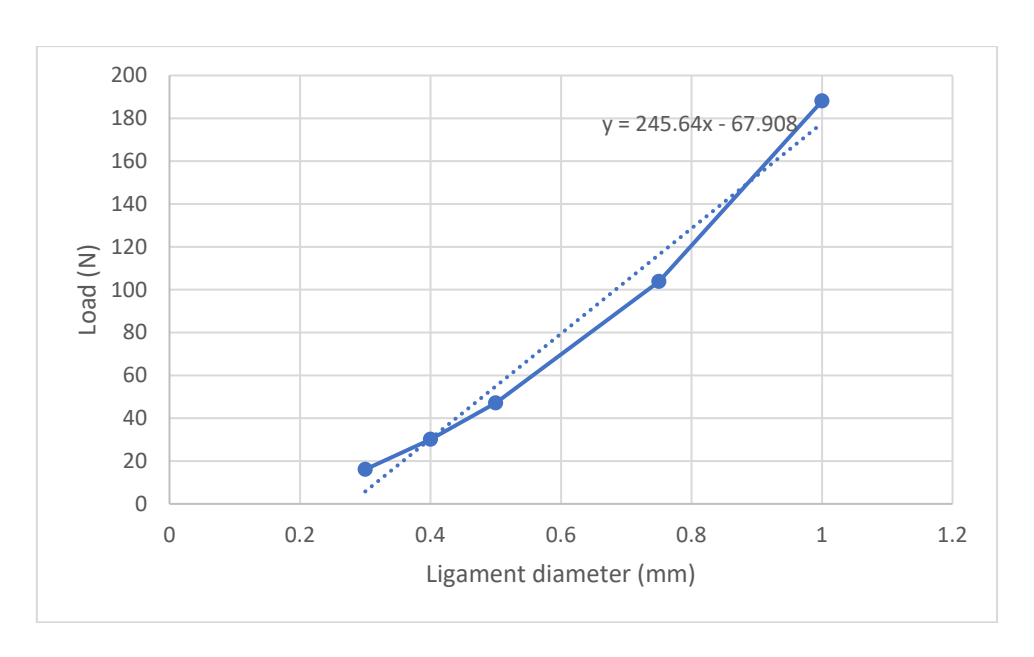


Figure 57 FE maximum load versus ligament diameter for all geometries

4.2 LATTICE MODEL

In previous work reported in NPL Report MAT 119 (4) a single unit cell of the lattice structure was modelled with a strut diameter of 0.3 mm and a unit cell width of 1 mm. The current lattice samples had a nominal diameter of 0.4 mm, so the original unit cell was scaled to increase the diameter to 0.4 mm. This action also increased the width of the unit cell, so adjustments needed to be made to the strut length and new 'rounded caps' were created to enable joining of the cells via nodes, see Figure 58 (a). The geometry was partitioned to allow for varying material properties along the strut, but hardness testing revealed little variation in properties, so these partitions weren't used in this instance. The geometry was meshed with quadratic tetrahedron, type C3D10, see Figure 58 (b). The material data used for the previous ligament modelling was also used for the lattice modelling.

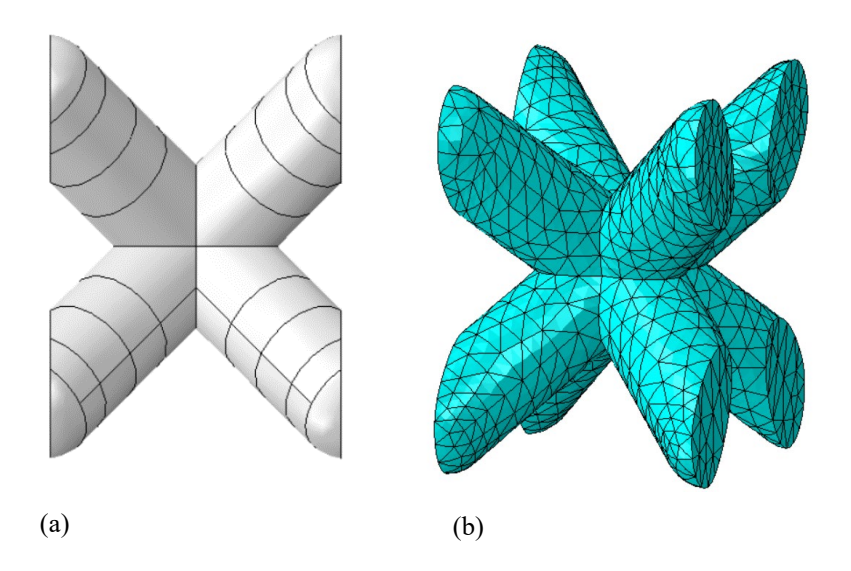


Figure 58 Single unit cell geometry (a) and meshed part (b)

For the single unit cell model, boundary conditions were applied to the model to simulate tensile loading. The nodes on the flat faces of the base of the geometry were fully constrained. The y-direction movement of the nodes on the top faces were tied to the displacement of a single reference node using an equation to allow output of the total force from this single node. The displacement of all nodes on these flat faces were constrained in the x- and z-directions, see Figure 59.

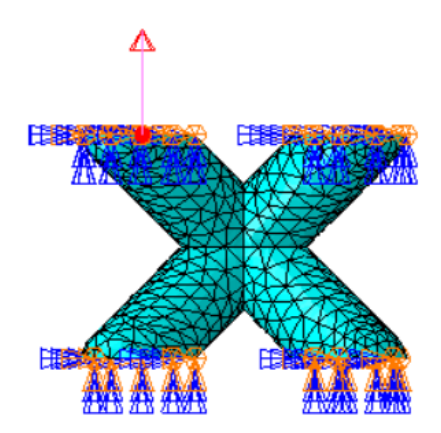


Figure 59 Boundary conditions applied to the single unit cell geometry

This single unit cell model was also used as the basis of a multi-unit cell model that would correlate with the additively manufactured lattice sample. The printed lattices were 9 units long starting and finishing from a central node rather than an outer edge. The mirror image tool in Abaqus CAE was used to create a line of 10 unit cells, which could then be cut down to the correct 9 unit geometry. Boundary conditions were applied in the same manner as for the single unit cell geometry, see Figure 60.

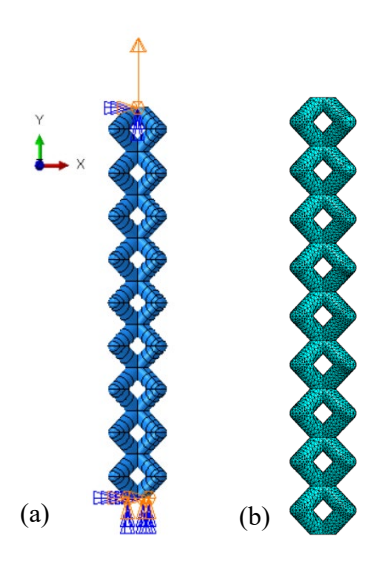


Figure 60 Lattice geometry showing (a) boundary conditions and (b) meshed geometry

This geometry was then used to create the larger lattice structure models. The models were set-up in the same manner as before. Figure 61 to Figure 64 shows the geometry and mesh for the $9 \times 2 \times 1$, $9 \times 5 \times 1$, $9 \times 5 \times 2$, $9 \times 5 \times 5$ geometries respectively. All geometries had a displacement of 0.4 mm applied.



Figure 61 Geometry and mesh of 9 x 2 x 1 geometry

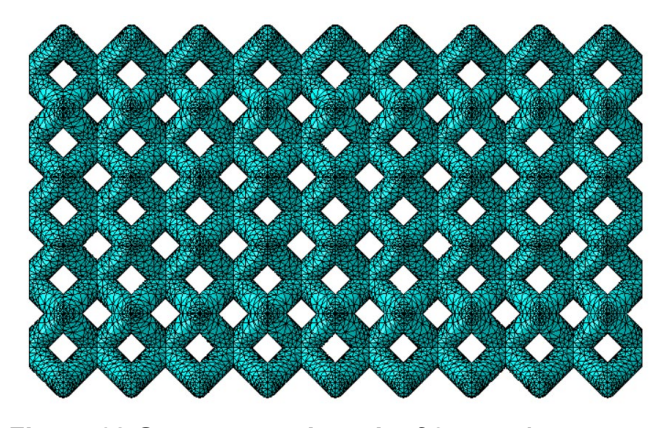


Figure 62 Geometry and mesh of 9 x 5 x 1 geometry

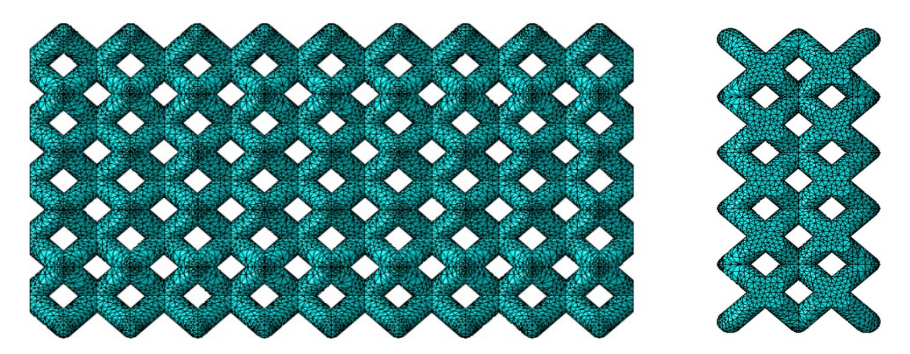


Figure 63 Geometry and mesh (front view and cross-section) of 9 x 5 x 2 geometry

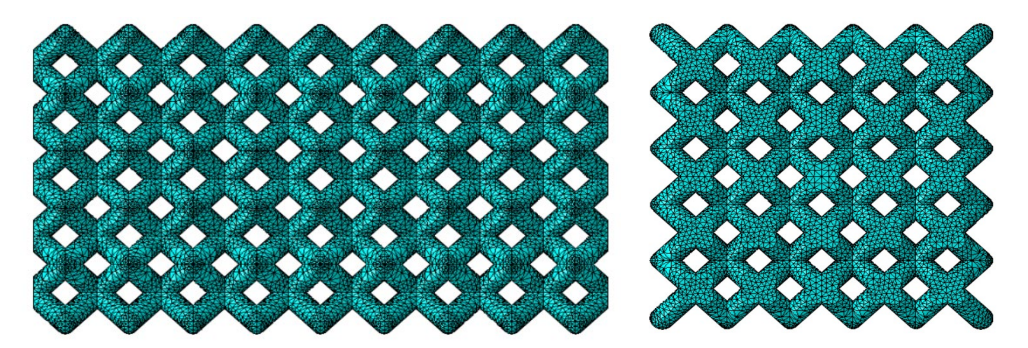


Figure 64 Geometry and mesh (front view and cross-section) of 9 x 5 x 5 geometry

An additional version of the $9 \times 5 \times 5$ model was created to investigate the effect of edge geometry. The above geometry in Figure 64 shows the lattice ending in nodes at the edges. The additional geometry created was offset to remove the neat, rounded nodes, Figure 65.

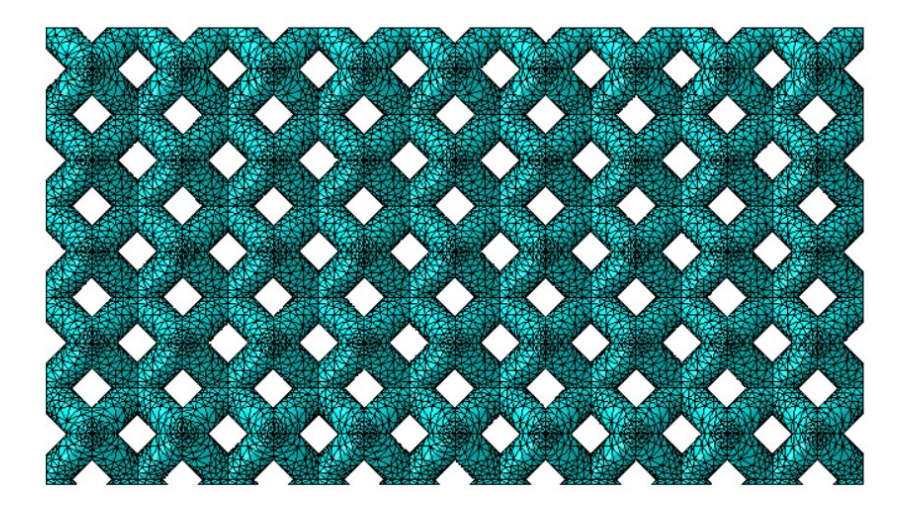


Figure 65 Geometry and mesh of the offset 9 x 5 x 5 geometry

Figure 66 shows the predicted load-displacement plots obtained from the six geometries presented above. As expected, wider samples with larger cross sections lead to higher predicted loads. When predictions from the two geometries shown in Figure 64 and Figure 65 were compared, there was very little different between them.

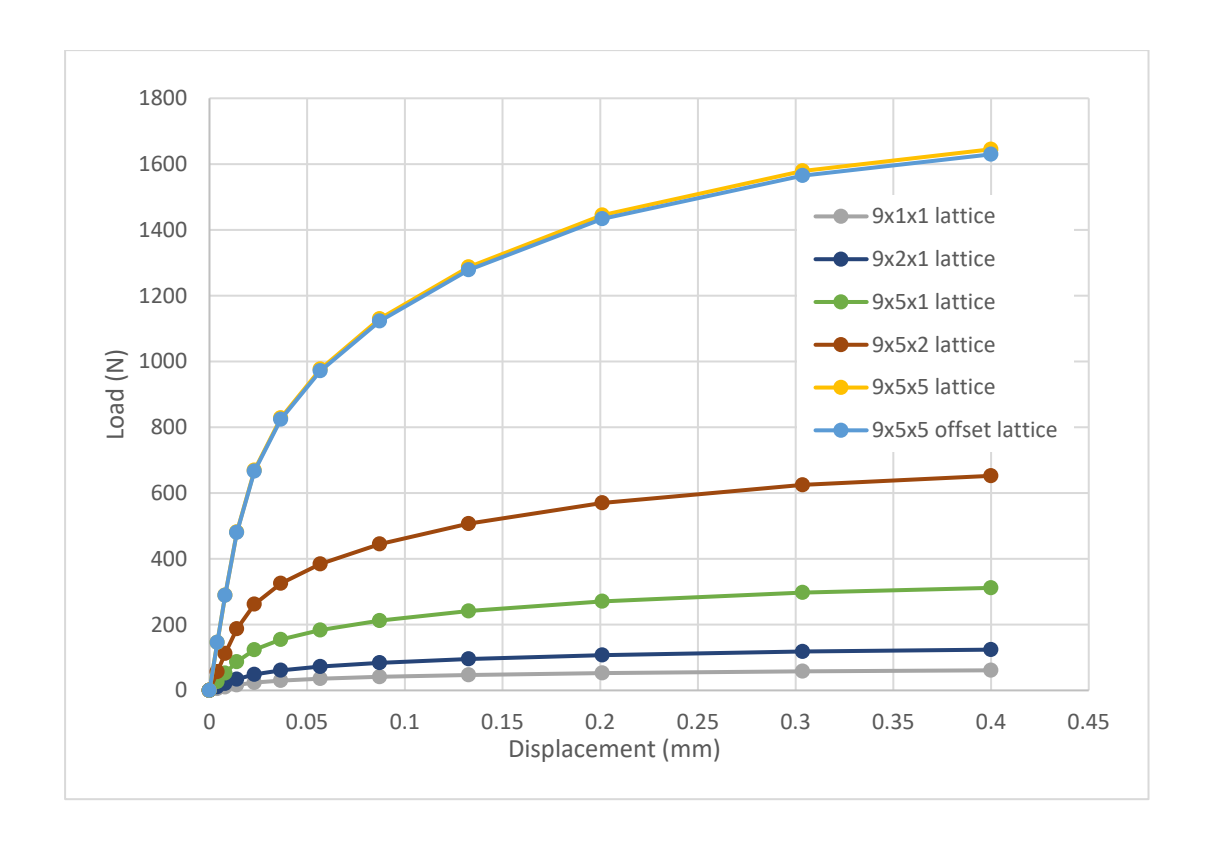


Figure 66 Load-displacement plots obtained from six lattice geometries with 0.4 mm diameter struts

Plotting the maximum predicted load at a displacement of 0.4 mm against the number of unit cells in the cross-section (e.g., 9 x 5 x 2 geometry has 10 unit cells in the cross-section) shows a linear trend, Figure 67.

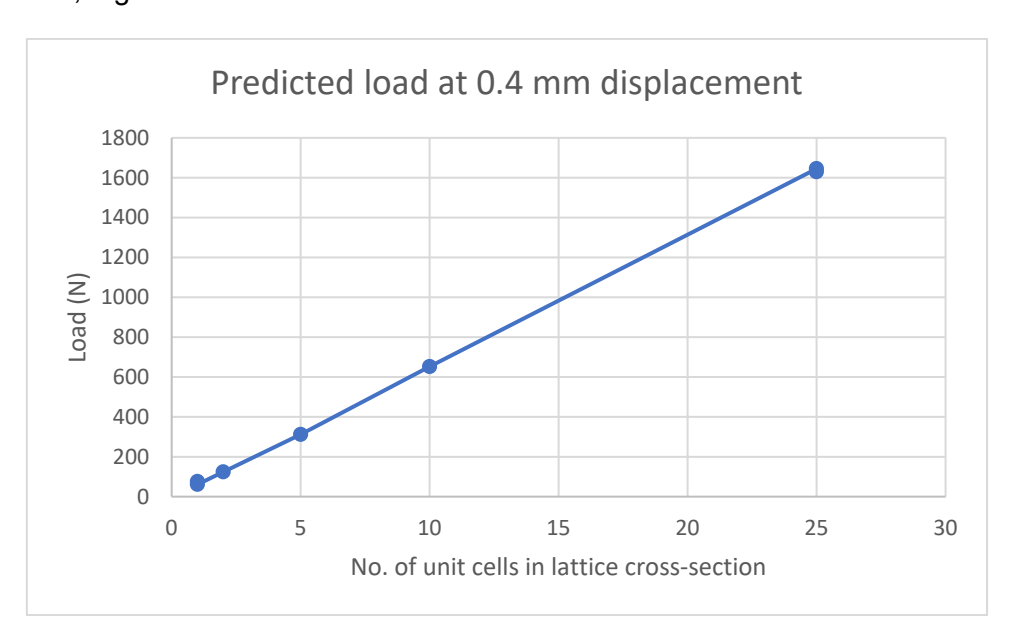


Figure 67 Predicted load at a displacement of 0.4 mm vs the number of unit cells in the crosssection

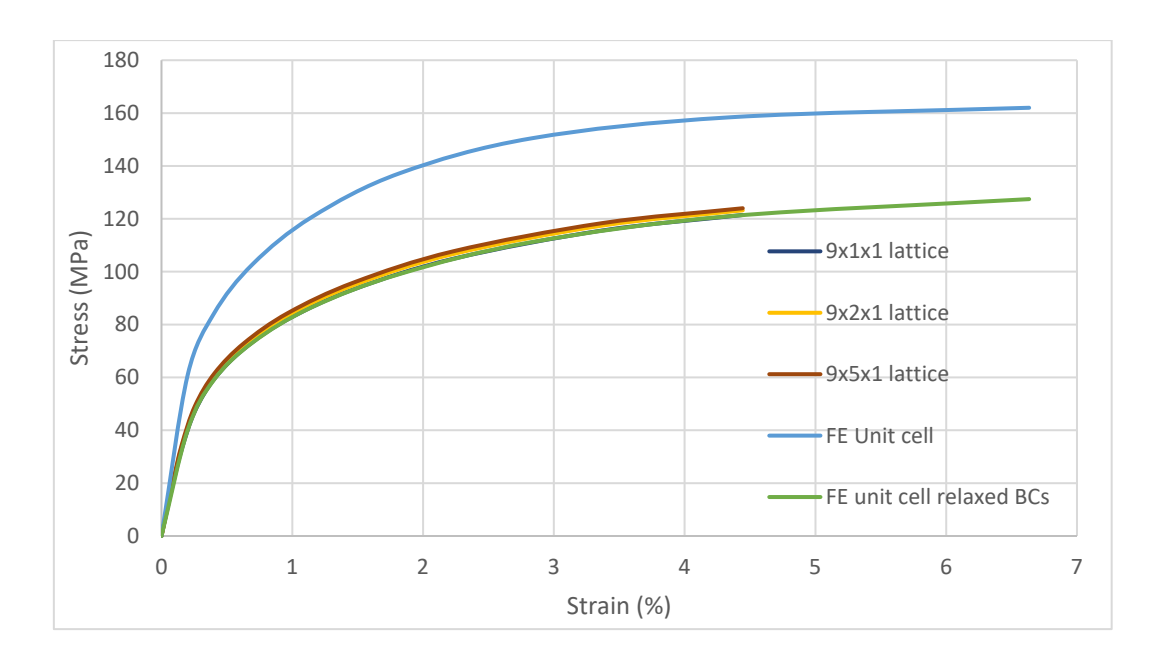


Figure 68 Stress-strain plots obtained from three lattice geometries and the single unit cell, all with 0.4 mm diameter struts

Figure 68 shows the stress-strain predictions for the three smaller, single layer, geometries, along with that for the single unit cell model described earlier. There is good correlation between the lattice curves. The high stiffness and predicted stress of the single unit cell geometry may be due to the model being over constrained. The free surfaces at the ends of the cell were constrained in the x and z directions, with a displacement applied to one end in the y direction. To investigate the effect of these constraints, a further model was created in which the free ends of the struts were allowed some movement in the x and z directions i.e., they could move closer to each other as the geometry is being 'stretched'. By relaxing the constraints of the single unit cell model, the predicted curve has aligned with the lattice data, Figure 68, showing a strong influence of applied boundary conditions to the predictions obtained.

Another consideration is the fact that the lattice models have boundary conditions applied to the end of the lattice section, to simulate the presence of the end tabs. To check that this is valid, the geometry of a single 9 x1 x 1 lattice was adapted to include end tab regions, Figure 69. Figure 70 confirms there is little difference between the two models and that the use of boundary conditions to represent the end tabs is reasonable.



Figure 69 Meshed geometry for 9 x 1 x 1 lattice with added end tabs

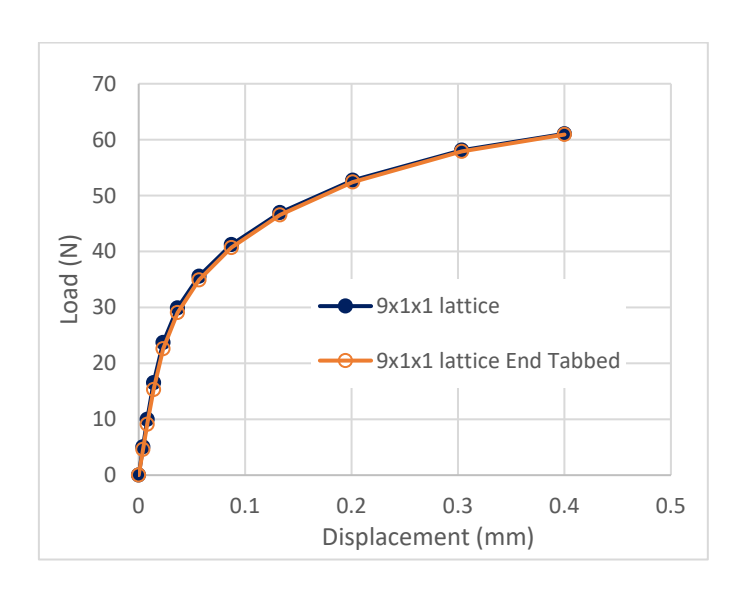


Figure 70 Load-displacement plots for 9 x 1 x 1 lattice with and without end tabs

When the predicted load-displacement curves were compared to the experimental data, it was found that the load was over predicted in all three cases, Figure 71. A possible reason for this is that the assumed 0.4 mm diameter might not be correct. A smaller diameter strut is likely to lead to smaller loads. Due to the printing process, there is likely to be some variation in strut shape which is not taken into account within the FE analysis.

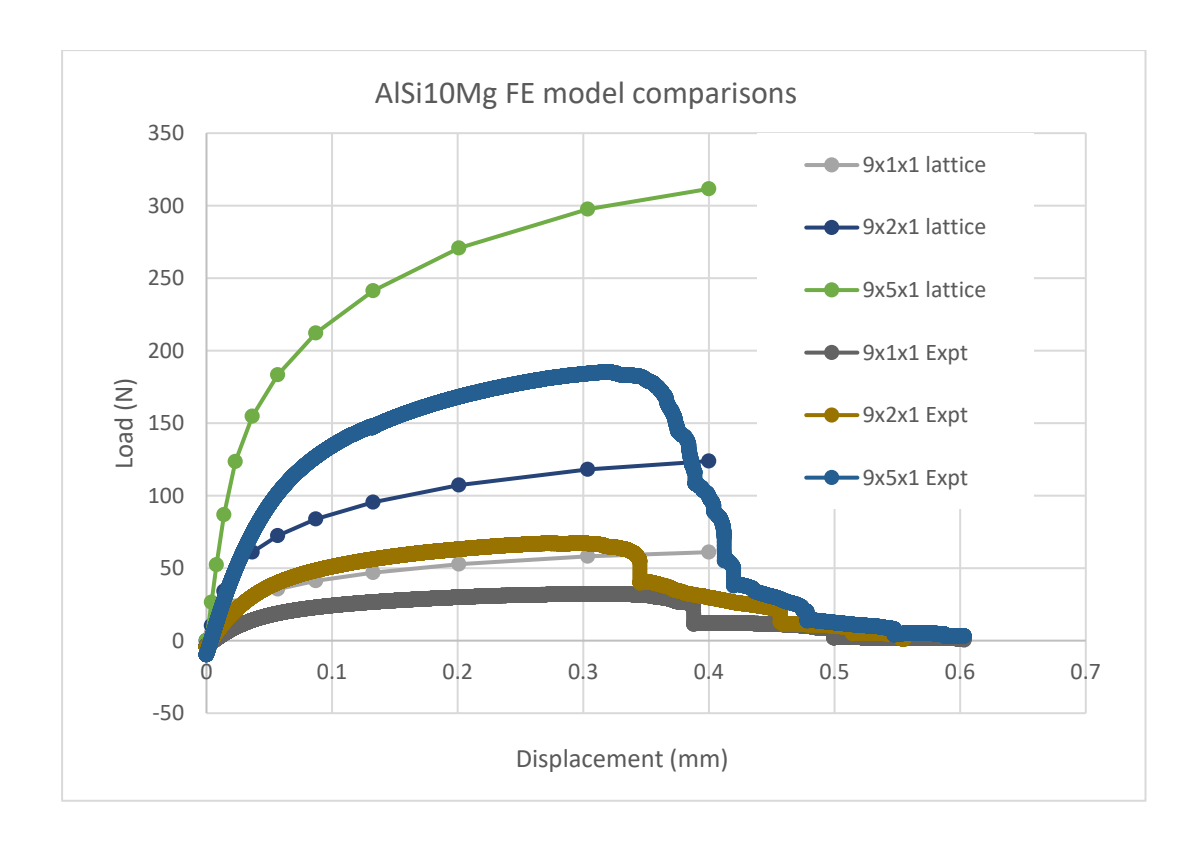


Figure 71 FE load-displacement plots compared to experimental data from three lattice geometries with 0.4 mm diameter struts

To investigate this theory a new suite of model geometries were created with a strut diameter of 0.3 mm, based on the single lattice geometry presented in previous work (NPL report MAT 119 ((4))). The initial geometry of the existing 0.3 mm lattice model was slightly different to the current model in that the lattice structure ended in 'free' struts, rather than a node. The geometry was adjusted so that all 0.3 mm models matched the 0.4 mm models. But to see if this offset in geometry had any effect on the performance of the lattice, the original geometry was also run. Figure 72 shows the current geometry (Figure 72 (a) ending at a node) and the offset geometry (Figure 72 (b) ending in 'free' struts).

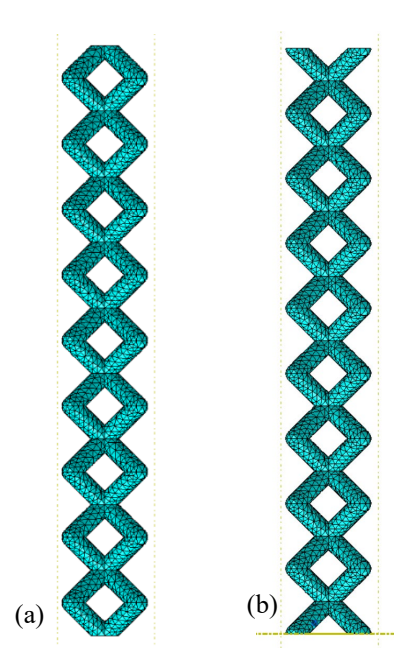


Figure 72 0.3 mm diameter lattice geometry showing (a) current configuration and (b) offset configuration for 9 x 1 x 1 lattice

The predictions from the 0.3 mm diameter analyses have been compared with the experimental data and the 0.4 mm strut lattice predictions in Figure 73 to Figure 75. The load-displacement predictions from the offset geometry show very little difference between the two configurations, Figure 73.

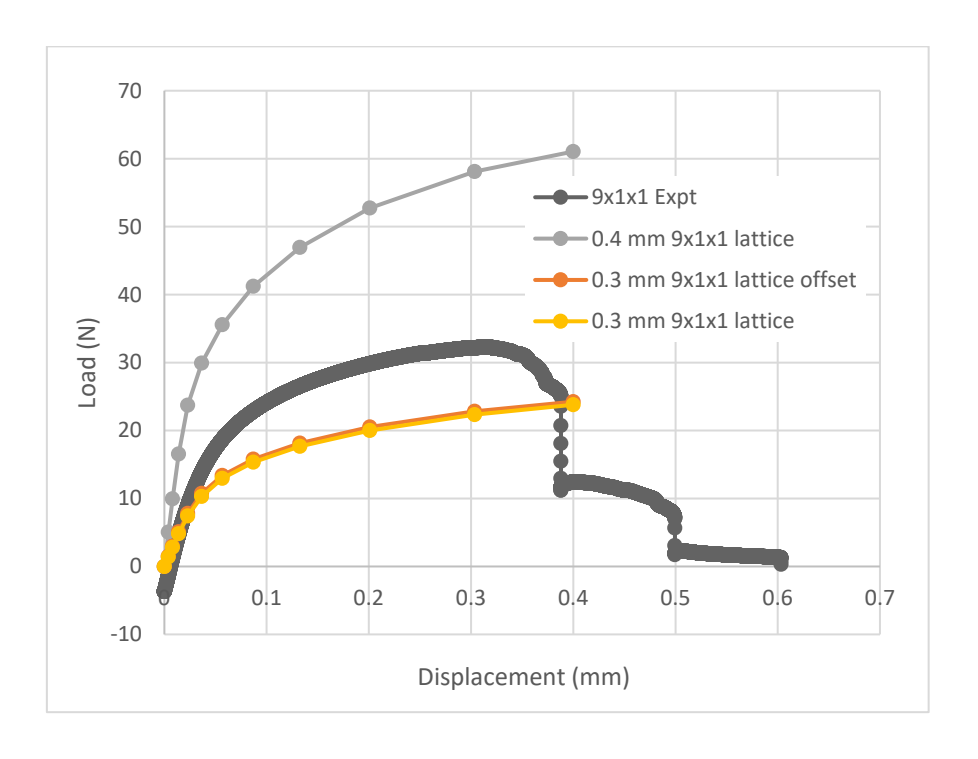


Figure 73 FE load-displacement plots compared to experimental data from 9 x 1 x 1 lattice with 0.3 mm and 0.4 mm diameter struts

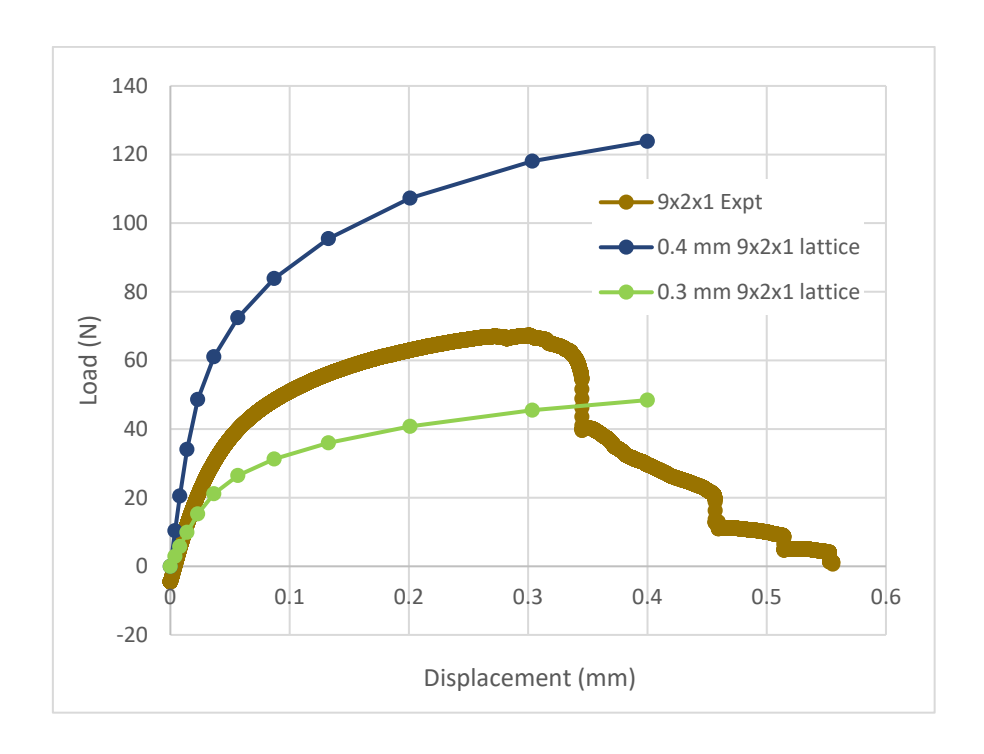


Figure 74 FE load-displacement plots compared to experimental data from 9 x 2 x 1 lattice with 0.3 mm and 0.4 mm diameter struts

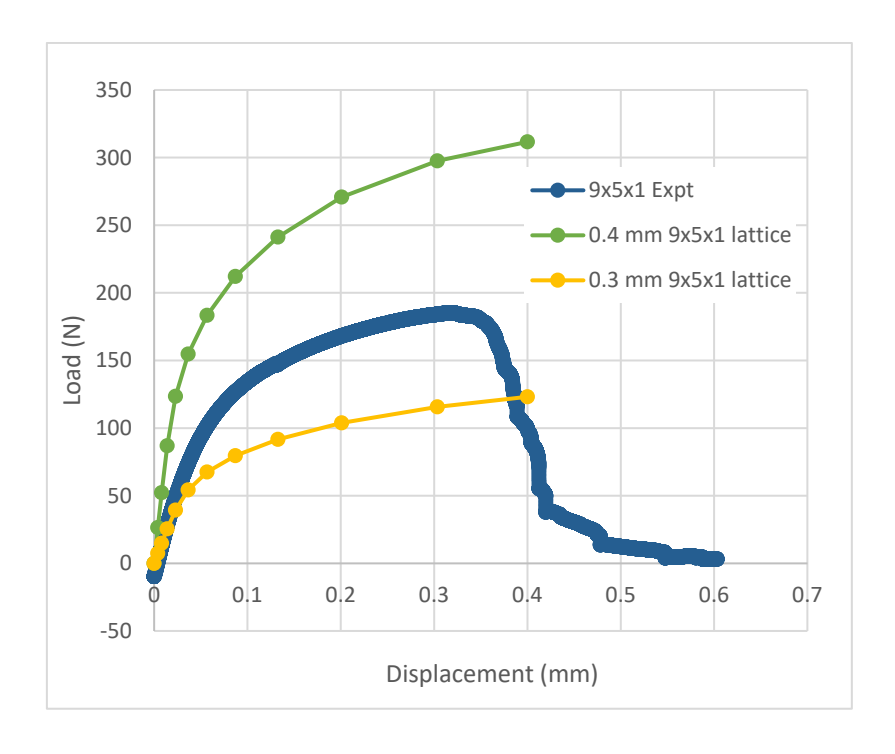


Figure 75 FE load-displacement plots compared to experimental data from 9 x 5 x 1 lattice with 0.3 mm and 0.4 mm diameter struts

The above graphs show that the FE predictions from the 0.3 mm and 0.4 mm diameter geometries bound the experimental data for all three geometries. This suggests that the actual diameter of the printed lattices is likely to be somewhere between the two. Rough measurements taken from the SEM images in Figure 43 gave diameters in the range 0.34 mm – 0.37 mm, which agrees with that expected from the comparison with the FE data. These

measurements need to be carried out more rigorously to confirm the average diameter in the lattices.

During experimental testing of the lattices, failure is seen to occur locally within one or two unit cells. The inclusion of failure mechanisms was outside the scope of this project, but it is possible to use FE analyses to investigate the effect of localised changes in material properties to simulate lower strength regions. This method is a simplified approach as the lower strength regions are present throughout the whole analysis rather than becoming weaker during the analysis.

This was investigated using the 9 x 1 x 1 geometry, with each unit cell within the geometry defined as an individual geometric set allowing different material properties to be defined for each cell. Three additional material property sets were defined. One had the modulus reduced to 50 GPa, but using the original hardening curve, the second had a 50 GPa modulus, and the yield stress values for the hardening curve were reduced by 25 MPa. The last case had a further reduced modulus (45 GPa) and the yield stresses reduced by 35 MPa. Figure 76 shows the 9 x 1 x 1 geometry with one material property set applied to the central unit cell, a different material set assigned to the unit cells either side of this, and a third material definition applied to the next two unit cells. The green unit cell was labelled 'C', the two cream ones labelled 'L1' and 'R1' and the two red ones labelled 'L2' and 'R2'. The remainder of the cells use the actual, measured material properties. This particular set up is for illustration only and is not a model that was run.



Figure 76 9 x 1 x 1 lattice geometry showing regions with different material properties assigned

Three base models were created:

- Central unit cell (C) with reduced properties, remainder assigned measured properties,
- Cells C, L1 and R1 with reduced properties, remainder assigned measured properties,
- Cells C, L1, L2, R1 and R2 with reduced properties, remainder assigned measured properties.

Each of these three base models were run three times, for the three reduced property cases defined.

The predicted load-displacement curves for all nine analyses are presented in Figure 77 along with the curve for the standard 9 x 1 x 1 lattice. It can be seen that reducing the properties in defined areas does reduce the predicted load. As the reduced properties are present throughout the analysis rather than developing during the test, the effect of reduced properties is seen within the whole load-displacement curve. This is in contrast to the experimental tests where individual unit cells become weaker and begin to fail during the test and result in a significant drop off in load at the later stages of the load-displacement curve.

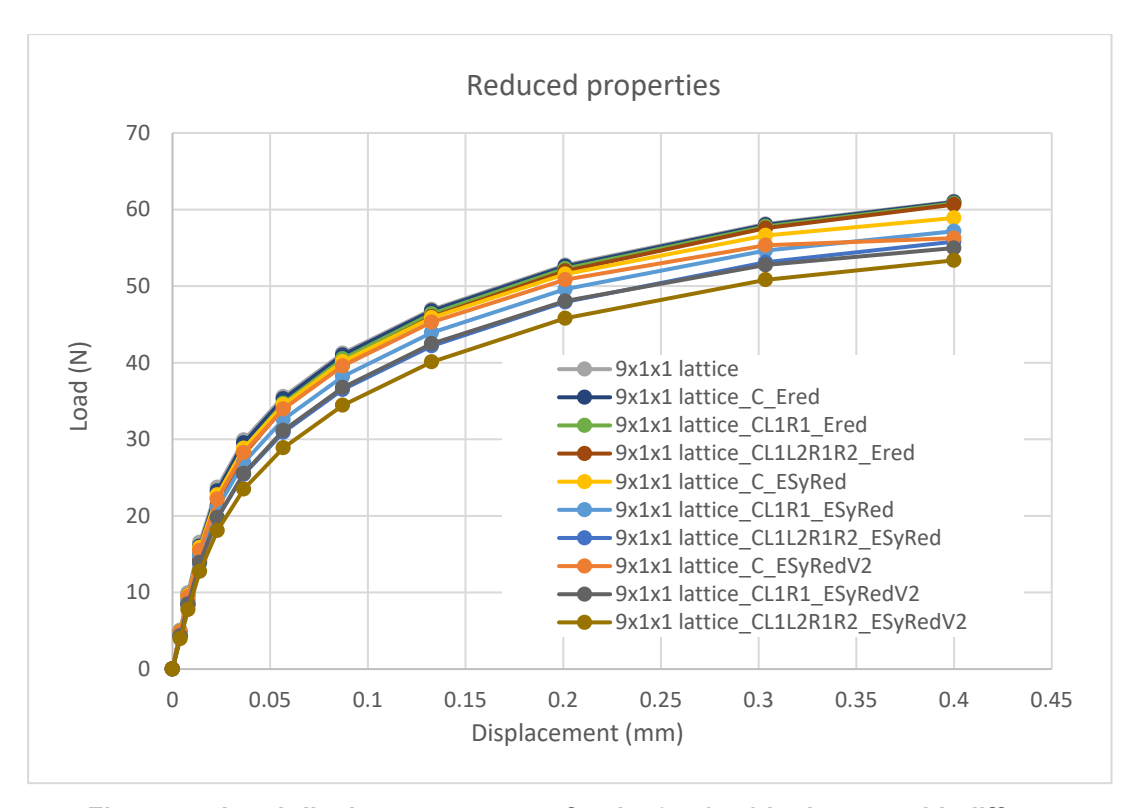


Figure 77 Load-displacement curves for the 9 x 1 x 1 lattice run with different material properties assigned

Experimentally, through the use of the Imetrum software, the strain within the lattice sample can be calculated over any specified range. Similarly, this can also be obtained from the FE data. These have been analysed for the intermediate property reduction case (modulus of 50 MPa, and stresses reduced by 25 MPa) to give strain calculated across the central cell, three central cells and five central cells, as well as the global strain. These curves have also been compared with a model run with only the actual measured properties assigned. Figure 78 shows the stress-strain curves for the case where the properties are reduced in the central cell only. In Figure 79, reduced properties have been applied to the central three cells, while in Figure 80 the central five cells have reduced properties. These graphs show that the predicted deformation is uniform within the reduced property regions. When increased deformation is occurring in only one cell, stress-strain curves are different for all the analysed strain regions. When increased deformation is occurring in three cells, the 1 cell and 3 cell strain are equivalent. The same is true for reduced properties in five cells where the 1 cell, 3 cell and 5 cell strains are now equivalent. This demonstrates that analysis of strain over different size regions can highlight exactly where additional deformation is occurring.

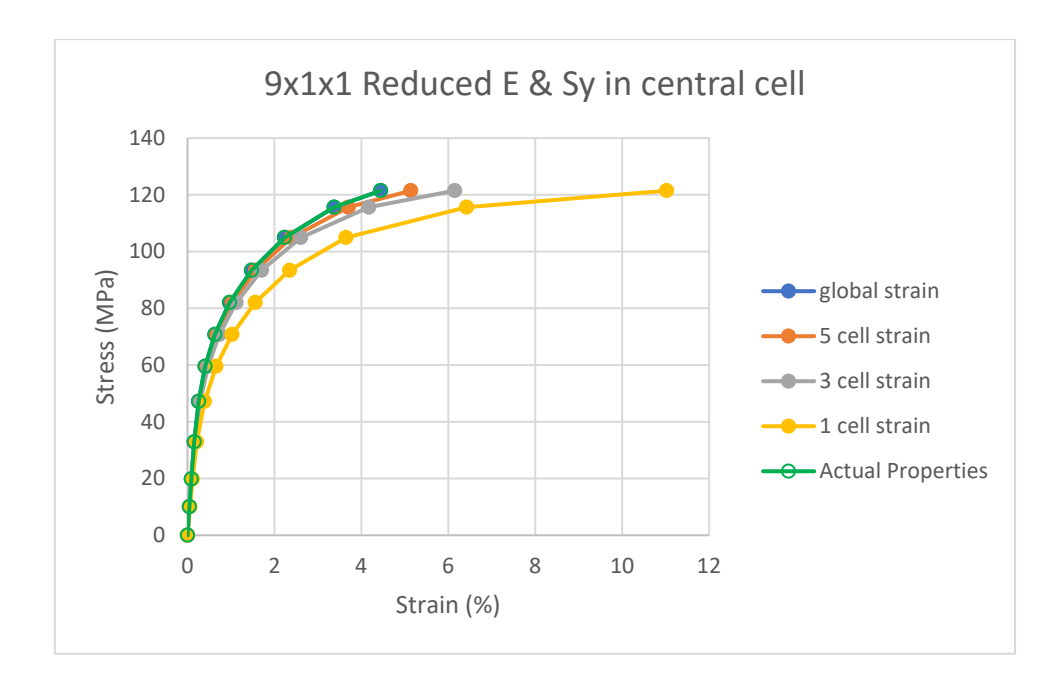


Figure 78 Stress-strain curves for the 9 x 1 x 1 lattice run with reduced modulus and stress values assigned to central cell only

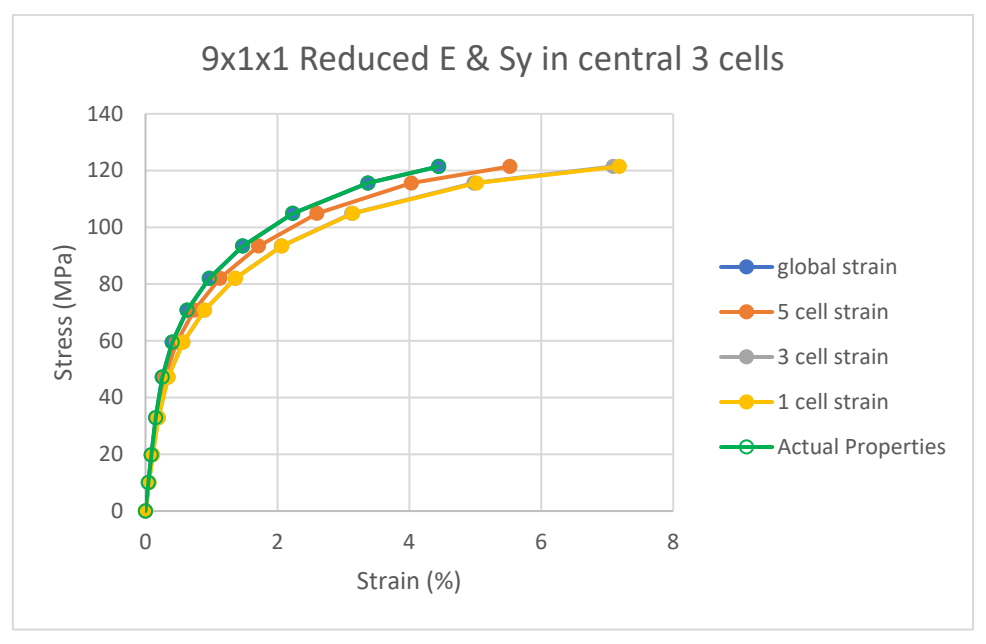


Figure 79 Stress-strain curves for the 9 x 1 x 1 lattice run with reduced modulus and stress values assigned to central three cell

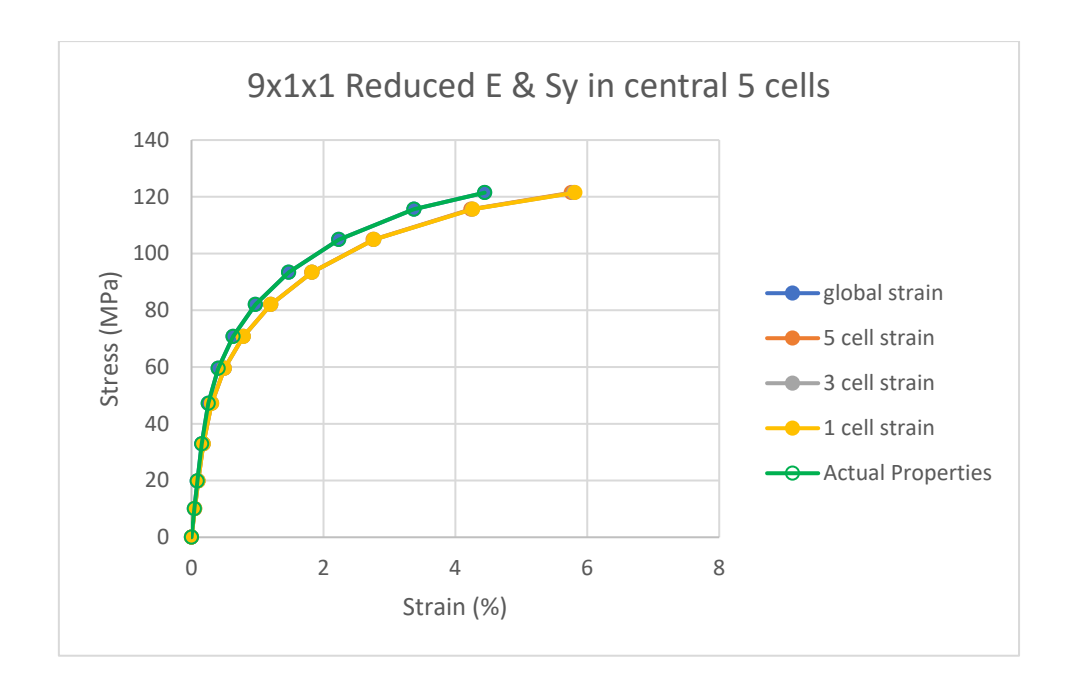


Figure 80 Stress-strain curves for the 9 x 1 x 1 lattice run with reduced modulus and stress values assigned to central five cell

5 DISCUSSION

A specimen design and testing approach has been developed an validated for the tensile testing of lattice structures. The ability to measure the properties of single struts, single lattice cells and multiple cell structures has been demonstrated.

Samples have been measured in both large scale universal test systems and in small scale in situ test rigs with the result comparing well. The use of in situ test rigs enables testing to be conducted in the SEM and so improved understanding of the mechanistic failure modes can be gained.

Nanonindentation testing has been used to determine the extent of variability in the elastic modulus in the lattice structure.

All this information has been used to develop, inform and validate FE models to help understand the tensile testing of lattice structures.

Single ligament FE models have been created for a range of ligament diameters. Good agreement is found between the FE predictions and the experimental data. The applicability of the boundary conditions used in the FEA has been verified.

A range of lattice geometries have been modelled with FEA using strut diameters of 0.3 mm and 0.4 mm. For the smaller lattice structures with a printed equivalent, the experimental data are bounded by the FE predictions from the two different diameter geometries. This suggests that the nominal diameter of the printed parts falls between 0.3 mm and 0.4 mm. Rough measurements from SEM images suggest the diameter is between 0.34 and 0.37 mm.

An investigation into the geometry edge effects was carried out, and changes to edge geometry and lattice/end tab connection geometry were found to have negligible effects.

The inclusion of failure mechanisms was outside the scope of this project, but it is possible to use FE analyses to investigate the effect of localised changes in material properties to simulate lower strength regions. This method is a simplified approach as the lower strength regions are present throughout the whole analysis rather than becoming weaker during the analysis. Lowering the modulus and yield stress values in the hardening curve had noticeable effects, but these were global effects on the whole load-displacement curve. This is in contrast to the experimental tests where individual unit cells become weaker and begin to fail during the test and result in a significant drop off in load at the later stages of the load-displacement curve.

It was demonstrated that the predicted deformation is uniform within the reduced property regions but this deformation is larger than the remaining lattice with the actual, measured properties. By analysing strains over different size areas it was found that when increased deformation is occurring in only one cell, stress-strain curves are different for all the analysed strain regions. When increased deformation is occurring in three cells, the 1 cell and 3 cell strain are equivalent. The same is true for reduced properties in five cells where the 1 cell, 3 cell and 5 cell strains are now equivalent. This demonstrates that analysis of strain over different size regions can highlight exactly where additional deformation is occurring.

6 REFERENCES

- 1. **Maconachie**, **T.** SLM lattice structures: Properties, performance, applications and challenges. *Mater Design.* 183, 2019, Vol. 108137.
- 2. **ASTM.** *Additive Manufacturing of metals Test artefacts Compression validation coupons for lattice designs.* s.l. : ASTM International, 2024. ISO/ASTM DIS 52959:2024(E).
- 3. **Alsalla, H, Hao, L and Smith, C.** Fracture toughness and tensile strength of 316L stainless steel cellualr lattice structures manufactured using the selective laser melting technique. *Mater Sci Eng.* 669, 2016.
- 4. Fry, A T, et al. Tensile propertuy measurement of lattice structures. s.l.: NPL, 2023. NPL Report MAT 119.
- 5. **Gavazzoni, M, et al.** Multiaxial static strength of a 3D printed metallic lattice structure exhibiting brittle behaviour. *Fatigue Fract Eng M.* 44, 2021, pp. 3499-3516.